9. Pellegrini G, Traverso CE, Franzi AT, et al. Long-term restoration of damaged corneal surfaces with autologous cultivated corneal epithelium. Lancet 1997;349:990–993.
10. Nakamura T, Inatomi T, Sotozono C, et al. Successful primary culture and autologous transplantation of corneal limbal epithelial cells from minimal biopsy for unilateral severe ocular surface disease. Acta Ophthalmol Scand 2004; 82:468–471.
11. Nishida K, Yamato M, Hayashida Y, et al. Functional bioengineered corneal epithelial sheet grafts from corneal stem cells expanded ex vivo on a temperature-responsive cell culture surface. Transplantation 2004;77:379–385.
12. Koizumi N, Inatomi T, Suzuki T, et al. Cultivated corneal epithelial transplantation for ocular surface reconstruction in acute phase of Stevens-Johnson syndrome. Arch Ophthalmol 2001;119:298–300.
13. Nakamura T, Endo K, Cooper LJ, et al. The successful culture and autologous transplantation of rabbit oral mucosal epithelial cells on amniotic membrane. Invest Ophthalmol Vis Sci 2003;44:106–116.
14. Nakamura T, Inatomi T, Stozono C, et al. Transplantation of cultivated autologous oral mucosal epithelial cells in patients with severe ocular surface disorders. Br J Ophthalmol 2004; 88:1280–1284.
15. Nishida K, Yamamoto M, Hayashi, Y et al. Corneal reconstruction with tissue-engineered cell sheets composed of autologous oral mucosal epithelium. N Engl J Med 2004;351:1187–1196.
16. Hayashida Y, Nishida K, Yamato M et al. Ocular surface reconstruction using autologous rabbit oral mucosal epithelial sheets fabricated ex vivo on a temperature-responsive culture surface. Invest Ophthalmol Vis Sci 2005;46:1632–1639.
17. Kinoshita S, Manabe R. Chemical burn. In: Brightbill FS, editor. Corneal surgery. St Louis: Mosby, 1986:370–379.
18. Gipson IK, Geggel HS, Spurr-Michaud SJ. Transplant of oral mucosal epithelium to rabbit ocular surface wounds in vivo. Arch Ophthalmol 1986;104:1529–1533.

REPORTING VISUAL ACUITIES

The AJO encourages authors to report the visual acuity in the manuscript using the same nomenclature that was used in gathering the data provided they were recorded in one of the methods listed here. This table of equivalent visual acuities is provided to the readers as an aid to interpret visual acuity findings in familiar units.

Table of Equivalent Visual Acuity Measurements

Snellen Visual Acuities			Decimal Fraction	LogMar
4 Meters	6 Meters	20 feet		
4/40	6/60	20/200	0.10	+1.0
4/32	6/48	20/160	0.125	+0.9
4/25	6/38	20/125	0.16	+0.8
4/20	6/30	20/100	0.20	+0.7
4/16	6/24	20/80	0.25	+0.6
4/12.6	6/20	20/63	0.32	+0.5
4/10	6/15	20/50	0.40	+0.4
4/8	6/12	20/40	0.50	+0.3
4/6.3	6/10	20/32	0.63	+0.2
4/5	6/7.5	20/25	0.80	+0.1
4/4	6/6	20/20	1.00	0.0
4/3.2	6/5	20/16	1.25	−0.1
4/2.5	6/3.75	20/12.5	1.60	−0.3
4/2	6/3	20/10	2.00	−0.3

From Ferris FL III, Kassoff A, Bresnick GH, Bailey I. New visual acuity charts for clinical research. Am J Ophthalmol 1982;94:91–96.

Unique Distribution of Thrombospondin-1 in Human Ocular Surface Epithelium

Eiichi Sekiyama,[1] Takahiro Nakamura,[1,2] Leanne J. Cooper,[3] Satoshi Kawasaki,[1] Junji Hamuro,[1] Nigel J. Fullwood,[3] and Shigeru Kinoshita[1]

Purpose. The study was conducted to elucidate the detailed expression pattern of angiogenesis-related factors in human ocular surface epithelium. The focus was factors with significantly higher gene expression in corneal epithelium (CE) than in conjunctival epithelium (CJE).

Methods. The relative gene expression of 36 angiogenesis-related factors was compared in human CE and CJE, by using the introduced amplified fragment-length polymorphism (iAFLP) method. Also examined were the expression patterns in the CE, limbal epithelium (LE), and CJE of factors with significantly higher expression in the CE, by using real-time PCR, in situ hybridization, immunohistochemistry, and immunoelectron microscopy.

Results. Only thrombospondin (TSP)-1 exhibited significantly higher expression in the CE. In situ hybridization and real-time PCR showed TSP-1 transcripts in the basal cells of the CE and LE. Compared with the CJE, they were significantly upregulated at those sites. Immunohistochemistry revealed that TSP-1 was strongly expressed in the basal region of the CE. Its expression was faint in LE and absent in CJE. Immunoelectron microscopy revealed that the CE and LE demonstrated TSP-1 labeling just below the epithelium, in the basal region of basal cells, and occasionally in the basal cell membrane. There was little or no labeling in the CJE.

Conclusions. In the human ocular surface epithelium, basal cells of the CE and LE, but not of the CJE, synthesize TSP-1. High levels of TSP-1 are present only just below the CE. Its unique distribution may be related to corneal avascularity and integrity. (*Invest Ophthalmol Vis Sci.* 2006;47:1352–1358) DOI:10.1167/iovs.05-1305

The corneal epithelium (CE) and conjunctival epithelium (CJE) are continuous, and together they comprise the ocular surface. Although both are stratified, squamous, nonkeratinizing epithelia that originate from surface ectoderm, they differ considerably in their characteristics and functions. For example, although some keratins are expressed in the CE and CJE as cytoskeletal proteins, they are of different subtypes.[1,2] In the CJE, but not the CE, goblet cells are interspersed between epithelial cells, and the tight junctions of the superficial cells render the CE impermeable to water-soluble substances. Consequently, compared with the CE, the CJE exhibits very poor barrier function.[3,4]

One of the major differences between the CE and CJE is the underlying vascular system. Although the connective tissue under the CJE is rich in vessels, the tissue under the normal CE is devoid of a vascular system. Corneal avascularity, necessary for good visual acuity, is attributable to the balanced expression of angiogenic and antiangiogenic factors.[5–10] Although the cornea is thought to produce and contain numerous antiangiogenic factors including thrombospondins,[5] pigment epithelial-derived factor,[6] and endostatin,[7] the mechanisms underlying the maintenance of corneal avascularity remain poorly understood.

To gain insight into angiogenesis-related corneal characteristics, we compared the gene expression patterns of 36 factors related to angiogenesis in the CE and CJE. We then investigated the detailed expression patterns in the ocular surface epithelium of factors with significantly higher expression in the CE than the CJE.

Materials and Methods

RNA Extraction from CE, LE, and CJE

Our study adhered to the tenets of the Declaration of Helsinki and was approved by the Institutional Review Board of Kyoto Prefectural University of Medicine. Human conjunctival epithelial cells were obtained from donors who provided prior informed consent.

Using donor tissues obtained from the Northwest Lions Eye Bank (Seattle, WA), we scraped the 4-mm diameter central region of the epithelium to obtain CE. For limbal epithelium (LE) we cut out the center part of the cornea and scraped the epithelium corresponding to the region of the palisades of Vogt ($n = 11$; mean age, 57.5 ± 6.4 years). After scraping the LE, we prepared sections of the remaining tissues and stained them with hematoxylin and eosin to ascertain that we harvested only LE and not CE. CJE cells from the bulbar conjunctiva of healthy volunteers were collected under topical anesthesia with 0.4% oxybuprocaine eye drops using a sterile nylon thread brush (Cytobrush Plus; Medscard Medical AB, Malmo, Sweden), as previously described ($n = 6$; mean age, 52 ± 5.8 years).[11]

After a 5-minute immersion of the CE, LE, and CJE at room temperature (RT) in acid phenol with guanidine isothiocyanate (TRIZOL reagent; Invitrogen Corp., Carlsbad, CA), total RNA was extracted and dissolved in distilled water according to the manufacturer's guidelines. To check its integrity, 1 μL of the RNA solution was electrophoresed on 1% agarose gels, the gels were stained (SYBR Green; Molecular Probes Inc., Eugene, OR), and 18S and 28S ribosomal RNA band fluorescence was quantified with a luminescent image analyzer (LAS1000; Fuji Film Medical Systems Inc., Stamford, CT). The remaining RNA was stored at −80°C until use.

Gene Expression Analysis by iAFLP

We examined the gene expression patterns in the CE and CJE of 36 angiogenesis-related factors (Table 1), using the introduced amplified fragment length polymorphism (iAFLP) method,[12,13] described else-

From the [1]Department of Ophthalmology, Kyoto Prefectural University of Medicine, Kyoto, Japan; the [2]Research Center for Regenerative Medicine, Doshisha University, Kyoto, Japan; and the [3]Institute of Environmental and Natural Sciences, Lancaster University, Lancaster, United Kingdom.

Submitted for publication October 2, 2005; revised November 10, 2005; accepted January 17, 2006.

Disclosure: **E. Sekiyama**, None; **T. Nakamura**, None; **L.J. Cooper**, None; **S. Kawasaki**, None; **J. Hamuro**, None; **N.J. Fullwood**, None; **S. Kinoshita**, None

The publication costs of this article were defrayed in part by page charge payment. This article must therefore be marked "*advertisement*" in accordance with 18 U.S.C. §1734 solely to indicate this fact.

Corresponding author: Eiichi Sekiyama, Department of Ophthalmology, Kyoto Prefectural University of Medicine, Kawaramachi Hirokoji, Kamigyo-ku, Kyoto 602-0841, Japan;
esekiyam@ophth.kpu-m.ac.jp.

Investigative Ophthalmology & Visual Science, April 2006, Vol. 47, No. 4

TABLE 1. Angiogenesis-Related Factors and Gene-Specific Primers

Thrombospondin-1*	5′-GTGATGAGTAAGGGTGGGGA-3′	TNF-alpha1*	5′-GCCAGATTCCAGATGTCAGGG-3′
Thrombospondin-3*	5′-GCCTCGCATGGATGTGTGAAT-3′	TNF-alpha2*	5′-GCCAAGGAGGAGTCATATCT-3′
VEGF	5′-GTCTTTCTGTCCGTCTGAGCGT-3′	HGF	5′-GTAAGGCTTTTTAGTATAAGA-3′
FGF-1	5′-GCAAACCAGGTCCCCAGATGA-3′	METH-1*	5′-GCCCCACCACAAGACAAGTGA-3′
FGF-2	5′-GTCCTACCTATTGCTTAAACT-3′	METH-2*	5′-GATGAAGTGAGGTCTGTTGA-3′
Angiopoietin-1	5′-GAGTAATGGAGTTTGTTTCTCA-3′	SDF-1	5′-GATACCACCAGGACCTTCTGT-3′
Angiopoietin-2	5′-GAGAATGCAGTTCCAAGATGA-3′	NK-4*	5′-GTCTCCCCAGGCTCCTCGGTT-3′
IL-1 alpha*	5′-GATGTAACATTATGGTCTGA-3′	GRO-beta*	5′-GCACACATACATTTCCCTGCC-3′
IL-1 beta*	5′-GCCTGGCTGATGGACAGGAGA-3′	IP-10*	5′-GCCCTCTGGTTTTAAGGAGAT-3′
IL-8*	5′-GTGGAACAAGGACTTGTGGA-3′	B 61	5′-GTACCTCCTGCCGTGTGGTGA-3′
IL-12 alpha	5′-GTCCACAGTAAATGTCAAAAATACT-3′	PF-4	5′-GCTATCAGTTGGGCAGTGGG-3′
IL-12 beta	5′-GTTTGCATAATAGGGACTGAT-3′	Somatostatin	5′-GGAAGAGAGATGGGGTGTGG-3′
TGF-beta 1	5′-GCAGCCTTGACCTCCCAGGAT-3′	Haptoglobin	5′-GAGCTCTTATCAAAGCTTAAGA-3′
TGF-beta 2*	5′-GCGTGTATCCATTTCCACCCT-3′	Erythropoietin*	5′-GTGGGGCCATTAGTTCCAGA-3′
TGF-beta 3*	5′-GTGTCCAAGGGGAAATATGA-3′	TIMP-1*	5′-GATACATCTTGGTCATCTTGA-3′
IGF	5′-GCATAGTTCATTAACTCTTTTACCA-3′	TIMP-2	5′-GTCAGGCCCTGCCCTAACCCA-3′
Angiogenin*	5′-GACGACGGAAAATTGACTGA-3′	G-CSF	5′-GTCCAAGGTGGGACCCAACTC-3′
Angiogenin-inhibitor*	5′-GACTGGCAGAAATAATGGGA-3′	CHM-1	5′-GCCCCCCACGGGTTCACAGA-3′

*Factors yielding products of the expected sizes.

where (n = 6). For validation and normalization, we examined the gene expression patterns of four keratins, 19 ribosomal protein subunits, and GAPDH by the same method. We used a pUC 19-base vector primer[14] to monitor the adequate synthesis and cleavage of cDNA on agarose gels. Extracted total RNA (1 μg) was annealed with a pUC 19-base vector primer (5 ng) in a total volume of 10 μL. After heat denaturation (70°C, 3 minutes), the reaction mixture that included 0.5 mM dNTP, 1× RT buffer (supplied with SuperScript II; Invitrogen), 15 mM dithiothreitol (DTT), and 0.1 U/mL of reverse transcriptase (SuperScript II; Invitrogen) was incubated for 60 minutes at 42°C. Second-strand synthesis then followed, in which 130 mL of second-strand reaction mixture was added, to yield a final concentration of 0.33 mM dNTP, 2.7 mM DTT, 1× *Escherichia coli* ligase buffer (supplied with *E. coli* ligase), 0.27 U/mL DNA polymerase I, 0.13 U/mL *E. coli* ligase, and 0.013 U/mL *E. coli* RNase H (all from Invitrogen). After purification by phenol-chloroform extraction and ethanol precipitation, cDNA was dissolved in 20 mL of distilled water, and 2.5 mL of the solution was stocked for electrophoresis.

To digest cDNA, 2 mL of 10× NEB3 buffer (supplied with *Mbo*I) and 5 units of *Mbo*I (New England Biolabs Ltd., Herfordshire, UK) were added. This was followed by incubation at 37°C for 60 minutes and heat inactivation at 70°C for 20 minutes. A small aliquot of the digested cDNA was electrophoresed on agarose gels along with stocked undigested cDNA, to check the quality of cDNA synthesis and *Mbo*I digestion. After checking, small aliquots (approximately 1:6) of all digested cDNAs were pooled to obtain a reference sample (control) to connect the data among the different sample sets. Then 100 picomoles of proper length-polymorphic (LP) adaptor (LP40, control; LP43, sample 1; LP46, sample 2; LP49, sample3; LP52, sample 4; LP55, sample 5), adenosine triphosphate (ATP), T4 DNA ligase (New England Biolabs, Ltd.), and 10× T4 ligase buffer (supplied with T4 DNA ligase, final concentration 1×) was added to the reaction mixture. After a 3-hour incubation at 16°C, all samples were pooled. They served as the template for PCR profiling. Using each template in the same ratio, PCR was performed with a gene-specific primer and a dye-labeled adaptor primer.[12] The conditions were preincubation at 94°C for 3 minutes and final extension at 72°C for 10 minutes, 30 cycles at 94°C for 30 seconds, 55°C for 30 seconds, and 72°C for 30 seconds. The PCR product was mixed with formamide loading buffer containing 1:4 volume of TAMRA-labeled size marker (GeneScan 350 TAMRA; Applied Biosystems [ABI], Foster City, CA). The mixture was denatured at 94°C for 2 minutes and then electrophoresed on a 10% acrylamide gel containing 6 M urea at a well-to-detector distance of 15 cm. We used an autosequencer (Prism377XL; ABI) and fragment analysis software (Genescan analysis software; ABI) to quantify each dye-labeled amplified fragment. Raw data were normalized by dividing the peak height of each target gene by the corresponding GAPDH gene peak height.

Real-Time PCR

We performed real-time PCR for TSP-1 (Prism 7000; ABI; n = 5). For reverse transcription we used 1 μg of total RNA, oligo (dT) primer, and RNase H-reverse transcriptase (SuperScript II; Invitrogen). Primers and probes for TSP-1 and β-actin were purchased from ABI. For relative quantification we used the ΔC_T method (ABI).[15] The C_T value is the fractional cycle number at which the amplified target amount reaches a fixed threshold of detectable fluorescence. The threshold was set in the midlinear phase of the amplification plot. To standardize the amount of sample cDNA added to each reaction, the amount of target gene in each sample was normalized to the endogenous control (β-actin) by subtracting the C_T of β-actin from the C_T of the target gene. Analyses were performed in a sequence detector (Prism 7000; ABI) using the accompanying data-analysis software.

In Situ Hybridization

Human TSP-1 cDNA, corresponding to base pairs 3874–4375 of the previously reported human TSP-1 cDNA (GenBank accession number NM_003246; http://www.ncbi.nlm.nih.gov/Genbank; provided in the public domain by the National Center for Biotechnology Information, Bethesda, MD), was subcloned into the pGEM-T vector (Promega, Madison, WI) and used for the generation of sense and antisense RNA probes. Digoxigenin (DIG)-labeled RNA probes were prepared with DIG RNA labeling mix (Roche, Basel, Switzerland).

Fresh human corneal-, limbal-, and conjunctival epithelia obtained from the eye bank were dissected, fixed, and embedded in paraffin by using proprietary procedures, and 6-μm sections were cut (n = 3; eyes aged 36.7 ± 16.5 years). They were deparaffinized with xylene, rehydrated with an ethanol series and phosphate-buffered saline (PBS), fixed with 4% paraformaldehyde in PBS (15 minutes), and then washed with PBS. Then the sections were treated with 10 μg/mL proteinase K in PBS (30 minutes, 37°C), washed with PBS, refixed with 4% paraformaldehyde in PBS, washed again with PBS, and placed in 0.2 M HCl for 10 minutes. After they were washed with PBS, the sections were acetylated by a 10-minute incubation in 0.1 M triethanolamine-HCl (pH 8.0) and 0.25% acetic anhydride. After they were again washed with PBS, they were dehydrated through an ethanol series. After 55°C, 16-hour hybridization to probes (100 ng/mL) in probe diluent (Genostaff, Tokyo, Japan), the sections were washed in 5× hybridization buffer equal to 5× SSC (HybriWash; Genostaff) at 55°C for 20 minutes and then in 50% formamide, 2× hybridization buffer (55°C, 20 minutes; HybriWash, Genostaff). This was followed by RNase treatment in 50 μg/mL RNase A in 10 mM Tris-HCl (pH 8.0), 1 M NaCl, and 1 mM EDTA. The sections were washed twice with 2× hybridization buffer (55°C, 20 minutes), twice with 0.2× of the buffer (55°C, 20 minutes), and once with TBST (Tris-buffered saline-0.1% Tween-20). After 30-

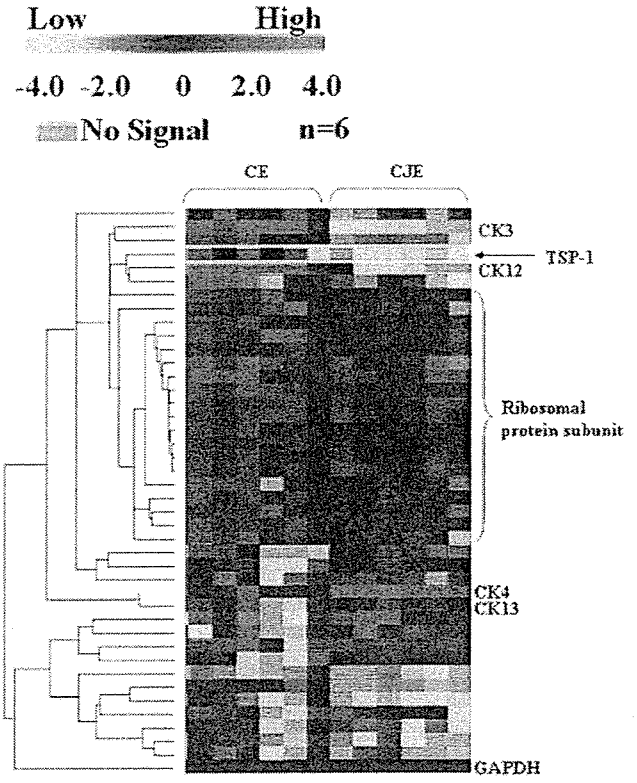

FIGURE 1. Hierarchical clustering of gene expression data obtained with the iAFLP method (n = 6). Each row represents an individual gene and each column an individual sample. Data are presented according to the color scale shown at *top left*. CK3, -4, -12, and -13 were used for validation in this experiment. TSP-1 (*yellow box*) was upregulated in the CE and was clustered close to CK3 and -12, which were also upregulated in the CE. CK4 and -13 were upregulated in the CJE and closely clustered. The ribosomal protein subunits showed similar expression patterns.

minute treatment with 0.5% blocking reagent (Roche) in TBST, the sections were incubated for 2 hours with anti-DIG AP conjugate (Roche) diluted 1:1000 with TBST. They were then washed twice with TBST and incubated in 100 mM NaCl, 50 mM $MgCl_2$, 0.1% Tween-20, and 100 mM Tris-HCl (pH 9.5). After an overnight color reaction with the BM purple alkaline phosphatase (AP) substrate (Roche), the sections were washed with PBS, dehydrated, and mounted on coverslipped glass slides (Malinol; Mutoh Chemical Co., Tokyo, Japan).

Immunohistochemistry for TSP-1

Residual tissues from penetrating keratoplasty (PKP) were obtained from the eye bank (n = 5, mean age: 49 ± 17.3 years). They were embedded in optimal cutting temperature (OCT) compound (Tissue-Tek; Miles, Inc., Elkhart, IN) and 8-μm-thick cryostat sections were cut so that the sections contained continuous epithelium from the central cornea to the limbal conjunctiva. The samples were examined immunohistochemically using our previously described method.[16] Briefly, after a 10-minute fixation in cold acetone, the sections were incubated for 20 minutes with 10% goat serum and 1% bovine serum albumin (BSA; Sigma-Aldrich, St. Louis, MO), incubated again at RT for 1 hour with two types of mouse anti-human primary antibody (catalog no. BA18, dilution: ×100; Oncogene, San Diego, CA; catalog no. T2905; dilution, ×100; Sigma-Aldrich), and washed three times for 10 minutes each in PBS. In control experiments, we replaced the primary antibody with identical concentrations of appropriate nonspecific normal mouse IgG (Dako, Kyoto, Japan).

After incubation with the primary antibody, the sections were washed with PBS containing 0.15% Triton X-100 and then incubated for 1 hour at RT with the appropriate secondary antibodies, FITC-conjugated anti-mouse antibodies (Molecular Probes, Inc.). After several washes with PBS, the sections were coverslipped with antifade mounting medium containing propidium iodide (Vectashield; Vector, Burlingame, CA) and examined by confocal microscope (Fluoview; Olympus, Tokyo, Japan).

Immunoelectron Labeling with TSP-1

Samples of tissues obtained from the U.S. Eye Bank were fixed in 2.5% paraformaldehyde in phosphate buffer (pH 7.2), washed three times in phosphate buffer containing 0.1 M glycine, and dehydrated through a graded series of ethanol (50%, 70%, 80%, and 90% ethanol solutions, 20 minutes at each concentration; n = 3, mean age, 37 ± 16.5 years). The samples were then transferred to resin (London Resin White; TAAB Laboratories, Aldermaston, UK) for infiltration, embedded in molds containing fresh resin, and polymerized at 50°C for 24 hours. Ultrathin sections were cut on an ultramicrotome (Ultracut E; Reichert, Vienna, Austria) and collected on gilded copper grids (G400; Agar Scientific, Stansted, UK).

We labeled for the primary mouse monoclonal antibody by first placing the tissue-bearing grids in droplets of 0.1 M glycine in PBS (×2, 10 minutes each) and then incubating them in droplets of normal goat serum (20 minutes at RT). After the excess goat serum was removed, the grids were incubated overnight at 4°C with the primary antibody (catalog no. BA18, dilution, ×50; Oncogene) in PBS buffer (pH 7.4) containing 1% BSA and 1% Tween-20 (buffer 1). In the control experiments, the primary antibody was replaced with nonspecific antibody.

The grids were washed three times for 8 minutes each in five droplets of buffer 1 and then five times (8 minutes each) in distilled water. They were subsequently transferred to the appropriate secondary antibody (1:50 dilution in PBS; pH 8.2) containing 1% BSA, 1% Tween-20, 1% normal goat serum, 1% fish gelatin, and 2% sodium chloride (buffer 2). Secondary goat anti-rabbit IgG or goat anti-mouse IgG gold-conjugated (5 nm) antibodies (British Biocell International, Cardiff, UK) were used to visualize the primary antibodies. The samples were incubated for 3 hours at room temperature, and the grids were washed three times for 8 minutes each in five droplets of buffer 2 and then five times (8 minutes each) in distilled water. After the final wash, the sections were counterstained in aqueous uranyl acetate for 1 hour and examined under a transmission electron microscope (JEM 1010; JEOL, Tokyo, Japan).

RESULTS

iAFLP Analysis

We compared the gene expression patterns of 36 major angiogenesis-related factors in human CE and CJE by using the iAFLP

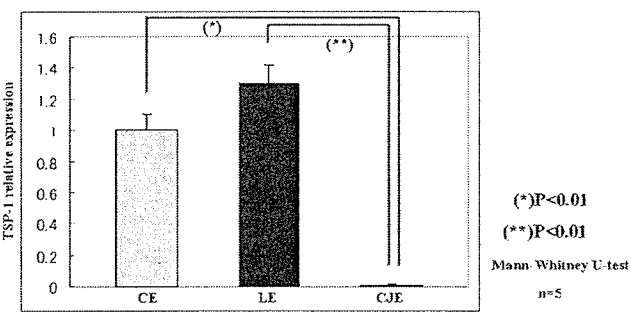

FIGURE 2. TSP-1 mRNA expression levels in the human CE, LE, and CJE, as determined by real-time PCR normalized to β-actin. The expression level of TSP-1 is significantly higher in the CE and LE than the CJE (n = 5, mean ± 0.08 and ± 0.13, respectively). The level of TSP-1 mRNA was slightly higher in the LE than the CE, but the difference was not statistically significant.

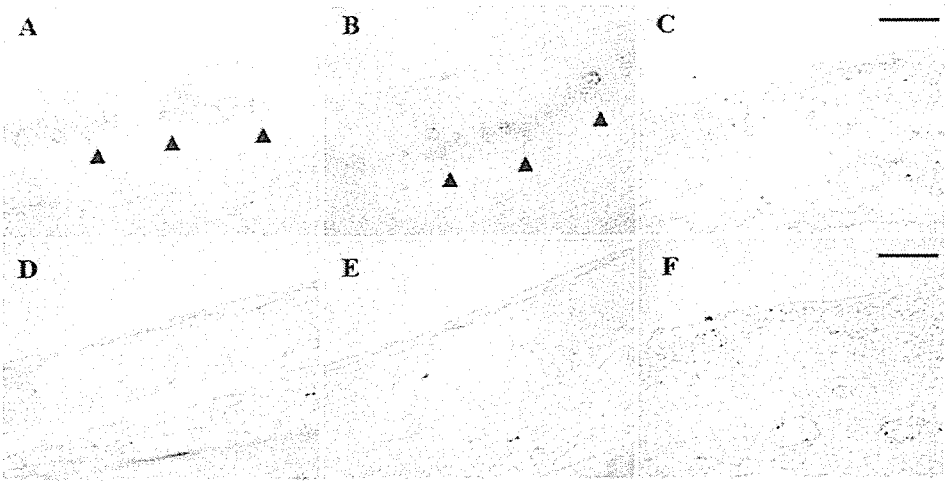

FIGURE 3. In situ hybridization of human TSP-1-specific mRNA in normal human ocular surface epithelium. The spatial anatomic distribution of TSP-1 transcripts was investigated in the CE (A), LE (B), and CJE (C). TSP-1 was expressed in corneal and limbal basal epithelial cells (A, B, *black arrowheads*). We did not detect TSP-1 transcripts in the CJE (C). (D–F) Sense RNA probes showed negligible levels of reactivity. Scale bars, 50 μm.

method. Of the 36 primers tested, 18 yielded products of the expected sizes, suggesting that the signals represented concentrations of target transcripts.

Among 36 factors, only TSP-1 was significantly upregulated in the CE (Fig. 1, yellow box). When we examined the expression pattern of keratins and ribosomal protein subunits used for validation, we found significant upregulation of CK3 and -12 in the CE, and of CK4 and -13 in the CJE and found similar expression patterns of 19 ribosomal protein subunits (Fig. 1). These results support the validity of the method used.

Real-Time PCR for TSP-1

The expression of TSP-1 mRNA in the CE, LE, and CJE ($n = 5$) was determined by real-time PCR. Compared with the CJE, mean TSP-1 mRNA was significantly upregulated in the CE and LE ($P < 0.01$, Mann-Whitney test). TSP-1 mRNA was slightly higher in the LE than the CE, although the difference was not statistically significant (Fig. 2).

In Situ Hybridization

In situ hybridization revealed the spatially restricted distribution of TSP-1 transcripts in the CE and LE, particularly in the basal epithelial cells (Figs. 3A, 3B, black arrowheads). We did not detect TSP-1 transcripts in any of the CJE layers (Fig. 3C). Sense RNA probes showed negligible levels of reactivity in all samples (Figs. 3D–F).

Immunohistochemistry for TSP-1

There was clear evidence of TSP-1 on the basement membrane side of the CE (Fig. 4A). Some patchy staining was detected in fibrous tissues and the corneal stroma below the LE (Fig. 4C, white arrows). Although we could detect moderate staining in the sclera distant from CJE, no staining was found in and just below the CJE (Fig. 4A). The area of TSP-1 expression in the ocular surface epithelium corresponded with Bowman's layer (Figs. 4A, 4C).

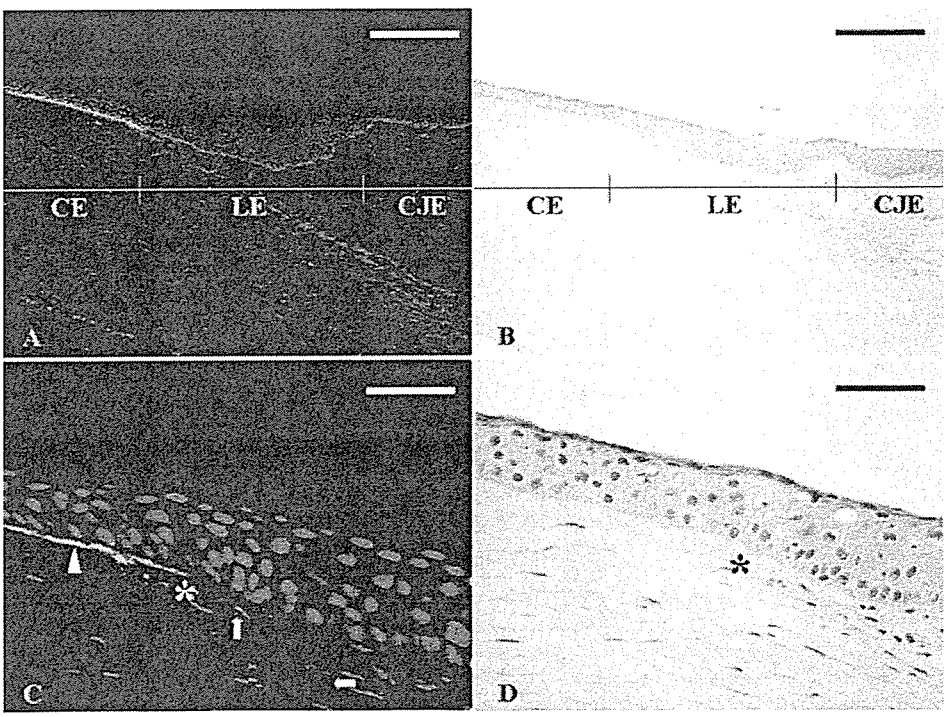

FIGURE 4. Representative immunohistochemical staining for TSP-1 (A) and hematoxylin-eosin staining in human ocular surface epithelium (CE, LE, and CJE; B). The enlarged micrographs show the area of transition between the CE and LE (C, D; *) termination of Bowman's layer. TSP-1 was present on the basal membrane side of the CE (A). Its distribution coincided with the area of Bowman's layer (C, *arrowhead*). Some patchy staining was detected in fibrous tissues and the corneal stroma below the LE (C, *arrows*). Although we detected moderate staining in the sclera distant from CJE, no staining was found in and just below the CJE (A). Scale bars: (A, B) 200 μm; (C, D) 50 μm.

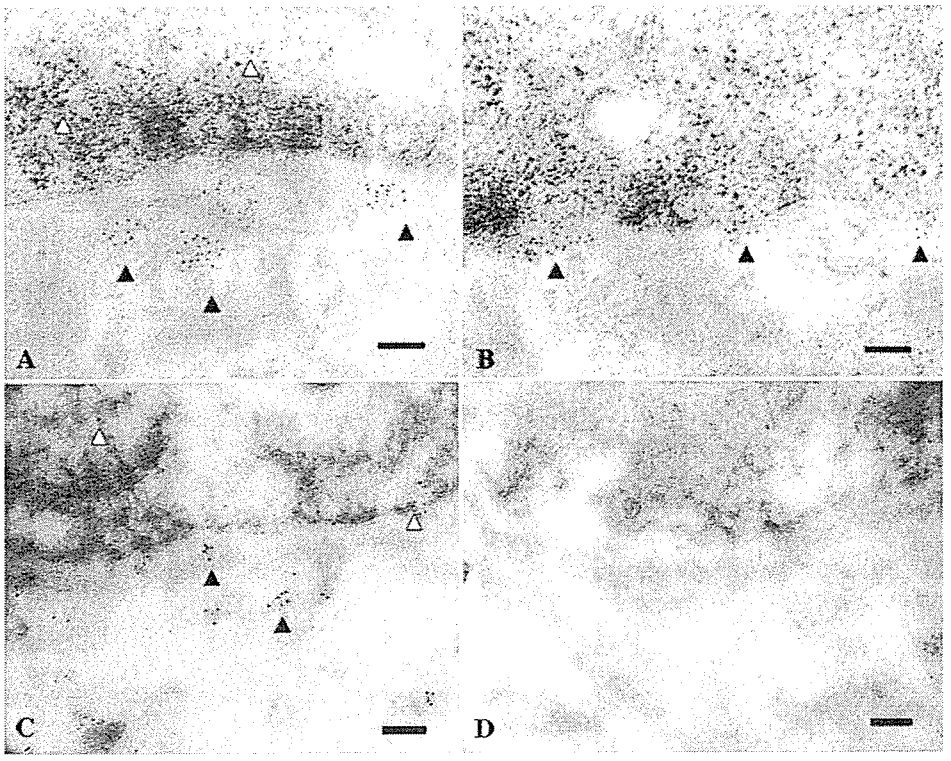

FIGURE 5. Transmission electron micrographs of the basal region of the CE (A, B), the LE (C), and the CJE (D). Significant labeling for TSP-1 was found in Bowman's layer (A, *black arrowheads*), inside basal cells (A, *white arrowheads*), and in the basal cell membrane (B, *black arrowheads*). There was some labeling just below the LE (C, *black arrowheads*) and inside basal cells (C, *white arrowheads*), but little or no labeling in the basal region of the CJE (D). The 5-nm gold particles appear as *black dots*. Scale bars, 100 nm.

Immunoelectron-Labeling with TSP-1

In the CE, Bowman's layer was strongly labeled for TSP-1 (Fig. 5A, black arrowheads). TSP-1 labeling was also found in the basal region of the basal cells (Fig. 5A, white arrowheads) and occasionally in the basal membrane of the epithelial cells (Fig. 5B, black arrowheads). In the LE, there was slight labeling just below the epithelial cells (Fig. 5C, white arrowheads), in the basal region of the basal cells, and occasionally in the basal membrane of the epithelial cells (Fig. 5C, black arrowheads). In contrast, the basal region of the CJE exhibited little or no labeling (Fig. 5D).

DISCUSSION

The cornea is one of the few avascular tissues in the adult body. Its avascularity is essential for corneal transparency and visual acuity. The mechanisms that maintain corneal avascularity and the characteristic angiogenesis-related differences between the cornea and conjunctiva remain poorly understood. Ours is the first report of the gene-expression patterns of major angiogenesis-related factors in the CE and CJE. We found that among 36 angiogenesis-related factors, TSP-1, one of the major antiangiogenic factors, was expressed at significantly higher levels in the CE.

TSP-1 was first identified as a platelet protein secreted on platelet activation[17,18] with a role in platelet aggregation.[18,19] TSP-1 has been described as a multifunctional protein that affects cell adhesion, migration, and proliferation[20,21] and plays a role in angiogenesis by exerting inhibitory effects on corneal neovascularization.[5,22,23] In mice, a deficit in a single antiangiogenic factor did not result in spontaneous corneal neovascularization.[24,25] We postulate that human corneal avascularity is also regulated by multiple antiangiogenic factors rather than a single one. Of interest, TSP-1, one of the major antiangiogenic factors contributing to corneal avascularity[5,6] was expressed at significantly higher levels in the human CE than in the CJE.

Our observation that TSP-1 transcripts were detected primarily in the basal cells of the CE and LE and that the protein was present in and just below the basal cells of both epithelia led us to postulate that TSP-1 was synthesized by basal corneal and limbal epithelial cells and that it was secreted primarily in the basal direction. TSP-1 is secreted by many types of cells including fibroblasts,[26,27] vascular endothelial cells,[26,27] smooth muscle cells,[26] macrophages, and monocytes.[28] Ours is the first documentation of its secretion in human ocular surface epithelium. In the current study, we provide evidence that in the human CE and LE, TSP-1 is secreted by basal cells, mainly toward the basal side.

Our immunoelectron microscopic study disclosed the detailed distribution of TSP-1 in the CE. Hiscott et al.[29] detected TSP-1 in the basal epithelial cell cytoplasm and basement membrane, but not within Bowman's layer. The presence of TSP-1 at the cell–matrix interface is not unexpected, because there is evidence that TSP-1 exists both as a secreted protein and as an insoluble extracellular matrix molecule[30,31] that binds to several macromolecules, such as heparin[32] and fibronectin,[33] and that it acts as an integrator of cell–matrix interactions.[34] We detected high levels of TSP-1 in Bowman's layer. TSP-1 has a high affinity for some collagens, particularly collagen type V,[35,36] and the main constituents of Bowman's layer are collagens I, III, and V.[37,38] We postulate that this explains its presence in Bowman's layer. The function of TSP-1 as an adaptor and modulator of cell–matrix interactions results in tissue remodeling and accelerated wound healing[20,21] and the transformation of latent TGF-β1 into an active form[39] that prompts the migration of corneal epithelial cells. Thus, TSP-1 in Bowman's layer may contribute to corneal epithelial cell migration and corneal avascularity. Studies are under way in our laboratory to elucidate the physiological implications of the observed TSP-1 distribution.

Although our immunohistochemical and immunoelectron microscopic studies detected TSP-1 in the CE, only slight immunohistochemical staining for TSP-1 was detected just below the LE. Immunoelectron labeling for TSP-1 in the LE confirmed that it was present in low amounts (Fig. 5C). We posit that although limbal basal epithelial cells secrete TSP-1 mainly toward the basal side, it diffuses rapidly into fibrous tissue, corneal stroma, or sclera because the area directly below the LE is devoid of Bowman's layer with an affinity for TSP-1. Regarding the fact that normal keratocytes do not secrete TSP-1,[40] we postulate that the staining in the sclera (Fig. 4A) below the CJE may have diffused from basal cells of the LE and/or fibroblasts in the connective tissues below the CJE. We thus suggest that TSP-1 located below the CE accumulates in Bowman's layer, whereas TSP-1 located below the LE diffuses into peripheral tissues.

In summary, in the human ocular surface epithelium, TSP-1 was secreted by corneal and limbal basal epithelial cells toward the basal side. In this respect, the LE and CE exhibited similar characteristics. In contrast to the LE, TSP-1 accumulated in Bowman's layer just below the CE. The expression pattern of TSP-1 in the CJE is different from the pattern noted in the CE and LE. The presence of TSP-1 in Bowman's layer may be related to corneal avascularity and the migration of corneal epithelial cells; however, the physiological relevance of its unique distribution remains to be elucidated. Investigations of the role of TSP-1 in the ocular surface epithelium are under way in our laboratory.

Acknowledgments

The authors thank Bernie Iliakis, Jeremy Shuman, and all the staff of the Northwest Lions Eye Bank (Seattle, WA) for providing corneas in good condition.

References

1. Schermer A, Galvin S, Sun TT. Differentiation-related expression of a major 64K corneal keratin in vivo and in culture suggests limbal location of corneal epithelial stem cells. *J Cell Biol.* 1986;103:49–62.
2. Eichner R, Bonitz P, Sun T-T. Classification of epidermal keratins according to their immunoreactivity, isoelectric point, and mode of expression. *J Cell Biol.* 1984;98:1388–1396.
3. Klyce SD, Crosson CE. Transport processes across the rabbit corneal epithelium: a review. *Curr Eye Res.* 1985;4:323–331.
4. Huang AJ, Tseng SC, Kenyon KR. Paracellular permeability of corneal and conjunctival epithelia. *Invest Ophthalmol Vis Sci.* 1989;30:684–689.
5. Cursiefen C, Masli S, Ng TF, et al. Roles of thrombospondin-1 and -2 in regulating corneal and iris angiogenesis. *Invest Ophthalmol Vis Sci.* 2004;45:1117–1124.
6. Murthy RC, McFarland TJ, Yoken J, et al. Corneal transduction to inhibit angiogenesis and graft failure. *Invest Ophthalmol Vis Sci.* 2003;44:1837–1842.
7. Shao C, Sima J, Zhang SX, et al. Suppression of corneal neovascularization by PEDF release from human amniotic membranes. *Invest Ophthalmol Vis Sci.* 2004;45:1758–1762.
8. Chang JH, Gabison EE, Kato T, Azar DT. Corneal neovascularization. *Curr Opin Ophthalmol.* 2001;12:242–249.
9. Lin HC, Chang JH, Jain S, et al. Matrilysin cleavage of corneal collagen type XVIII NC1 domain and generation of a 28-kDa fragment. *Invest Ophthalmol Vis Sci.* 2001;42:2517–2524.
10. Folkman J. Endogenous angiogenesis inhibitors. *APMIS.* 2004;112:496–507.
11. Tsubota K, Ugajin S, Hasegawa T, Kajiwara K. Conjunctival brush cytology. *Acta Cytol.* 1990;34:233–235.
12. Kawamoto S, Ohnishi T, Kita H, Chisaka O, Okubo K. Expression profiling by iAFLP: a PCR-based method for genome-wide gene expression profiling. *Genome Res.* 1999;9:1305–1312.
13. Kawasaki S, Kawamoto S, Yokoi N, et al. Up-regulated gene expression in the conjunctival epithelium of patients with Sjogren's syndrome. *Exp Eye Res.* 2003;77:17–26.
14. Okubo K, Hori N, Matoba R, et al. Large scale cDNA sequencing for analysis of quantitative and qualitative aspects of gene expression. *Nat Genet.* 1992;2:173–179.
15. Gipson IK, Spurr-Michaud S, Argueso P, Tisdale A, Ng TF, Russo CL. Mucin gene expression in immortalized human corneal-limbal and conjunctival epithelial cell lines. *Invest Ophthalmol Vis Sci.* 2003;44:2496–2506.
16. Nakamura T, Nishida K, Dota A, Kinoshita S. Changes in conjunctival clusterin expression in severe ocular surface disease. *Invest Ophthalmol Vis Sci.* 2002;43:1702–1707.
17. Baenziger NL, Brodie GN, Majerus PW. Isolation and properties of a thrombin-sensitive protein of human platelets. *J Biol Chem.* 1972;247:2723–2731.
18. Gartner TK, Phillips DR, Williams DC. Expression of thrombin-enhanced platelet lectin activity is controlled by secretion. *FEBS Lett.* 1980;113:196–199.
19. Phillips DR, Jennings LK, Prasanna HR. Ca2+-mediated association of glycoprotein G (thrombin sensitive protein, thrombospondin) with human platelets. *J Biol Chem.* 1980;255:11629–11632.
20. Uno K, Hayashi H, Kuroki M, et al. Thrombospondin-1 accelerates wound healing of corneal epithelia. *Biochem Biophys Res Commun.* 2004;315:928–934.
21. Greenwood JA, Murphy-Ullrich JE. Signaling of de-adhesion in cellular regulation and motility. *Microsc Res Tech.* 1998;43:420–432.
22. Tuszynski GP, Nicosia RF. The role of thrombospondin-1 in tumor progression and angiogenesis. *Bioessays.* 1996;18:71–76.
23. Castle VP, Dixit VM, Polverini PJ. Thrombospondin-1 suppresses tumorigenesis and angiogenesis in serum- and anchorage-independent NIH 3T3 cells. *Lab Invest.* 1997;77:51–61.
24. Bugge TH, Flick MJ, Daugherty CC, Degen JL. Plasminogen deficiency causes severe thrombosis but is compatible with development and reproduction. *Genes Dev.* 1995;9:794–807.
25. Soloway PD, Alexander CM, Werb Z, Jaenisch R. Targeted mutagenesis of Timp-1 reveals that lung tumor invasion is influenced by Timp-1 genotype of the tumor but not by that of the host. *Oncogene.* 1996;13:2307–2314.
26. Raugi GJ, Mumby SM, Abbott-Brown D, Bornstein P. Thrombospondin: synthesis and secretion by cells in culture. *J Cell Biol.* 1982;95:351–354.
27. Jaffe EA, Ruggiero JT, Leung LK, Doyle MJ, McKeown-Longo PJ, Mosher DF. Cultured human fibroblasts synthesize and secrete thrombospondin and incorporate it into extracellular matrix. *Proc Natl Acad Sci USA.* 1983;80:998–1002.
28. Jaffe EA, Ruggiero JT, Falcone DJ. Monocytes and macrophages synthesize and secrete thrombospondin. *Blood.* 1985;65:79–84.
29. Hiscott P, Seitz B, Schlötzer-Schrehardt U, Naumann GO. Immunolocalisation of thrombospondin 1 in human, bovine and rabbit cornea. *Cell Tissue Res.* 1997;289:307–310.
30. Lahav J. The functions of thrombospondin and its involvement in physiology and pathophysiology. *Biochim Biophys Acta.* 1993;1182:1–14.
31. Bornstein P. Diversity of function is inherent in matricellular proteins: an appraisal of thrombospondin 1. *J Cell Biol.* 1995;130:503–506.
32. Raugi GJ, Mumby SM, Ready CA, Bornstein P. Location and partial characterization of the heparin-binding fragment of platelet thrombospondin. *Thromb Res.* 1984;36:165–175.
33. Lahav J, Lawler J, Gimbrone MA. Thrombospondin interactions with fibronectin and fibrinogen: mutual inhibition in binding. *Eur J Biochem.* 1984;145:151–156.
34. Murphy-Ullrich JE. The de-adhesive activity of matricellular protein: is intermediate cell adhesion an adaptive state (review)? *J Clin Invest.* 2001;107:785–790.
35. Takagi J, Fujisawa T, Usui T, Aoyama T, Saito Y. A single chain 19-kDa fragment from bovine thrombospondin binds to type V collagen and heparin. *J Biol Chem.* 1993;268:15544–15549.

36. Galvin NJ, Vance PM, Dixit VM, Fink B, Frazier WA. Interaction ofhuman thrombospondin with types I-V collagen: direct binding and electron microscopy. *J Cell Biol.* 1987;104:1413–1422.
37. Marshall GE, Konstas AG, Lee WR. Immunogold fine structural localization of extracellular matrix components in aged human cornea. I. Types I-IV collagen and laminin. *Graefes Arch Clin Exp Ophthalmol.* 1991;229:157–163.
38. Marshall GE, Konstas AG, Lee WR. Immunogold fine structural localization of extracellular matrix components in aged human cornea. II. Collagen types V and VI. *Graefes Arch Clin Exp Ophthalmol.* 1991;229:164–171.
39. Schults-Cherry S, Lawler J, Murphy-Ullrich JE. The type I repeats of thrombospondin 1 activate latent transforming growth factor-β. *J Biol Chem.* 1994;269:26783–26788.
40. Armstrong DJ, Hiscott P, Batterbury M, Kaye S. Corneal stromal cells (keratocytes) express thrombospondins 2 and 3 in wound repair phenotype. *Int J Biochem Cell Biol.* 2002;34:588–593.

Neural conversion of ES cells by an inductive activity on human amniotic membrane matrix

Morio Ueno*†‡, Michiru Matsumura*, Kiichi Watanabe*, Takahiro Nakamura†, Fumitaka Osakada*§, Masayo Takahashi§, Hiroshi Kawasaki¶, Shigeru Kinoshita†, and Yoshiki Sasai*‖

*Organogenesis and Neurogenesis Group, RIKEN Center for Developmental Biology, Kobe 650-0047, Japan; †Department of Ophthalmology, Kyoto Prefectural University of Medicine, Kyoto 602-8566, Japan; §Translational Research Center, Kyoto University Hospital, Kyoto 606-8507, Japan; and ¶Department of Molecular and System Neurobiology, Graduate School of Medicine, University of Tokyo, Tokyo 113-0033, Japan

Edited by Igor B. Dawid, National Institutes of Health, Bethesda, MD, and approved May 1, 2006 (received for review January 6, 2006)

Here we report a human-derived material with potent inductive activity that selectively converts ES cells into neural tissues. Both mouse and human ES cells efficiently differentiate into neural precursors when cultured on the matrix components of the human amniotic membrane in serum-free medium [amniotic membrane matrix-based ES cell differentiation (AMED)]. AMED-induced neural tissues have regional characteristics (brainstem) similar to those induced by coculture with mouse PA6 stromal cells [a common method called stromal cell-derived inducing activity (SDIA) culture]. Like the SDIA culture, the AMED system is applicable to the *in vitro* generation of various CNS tissues, including dopaminergic neurons, motor neurons, and retinal pigment epithelium. In contrast to the SDIA method, which uses animal cells, the AMED culture uses a noncellular inductive material derived from an easily available human tissue; therefore, AMED should provide a more suitable and versatile system for generating a variety of neural tissues for clinical applications.

neural differentiation | extracellular matrix | dopaminergic neuron | retinal pigment epithelium | lens

Over the past several years, much progress has been made in the *in vitro* control of neural differentiation of ES cells. Neural conversion of mouse ES (mES) cells can be induced *in vitro* by several methods: retinoic acid (RA) treatment of embryoid bodies (EB) (1, 2), multistep-induction/selection culture (3), serum-free adherent monoculture (4), serum-free suspension culture (5), and feeder cell-dependent induction culture (6–9). Each method has its own advantages and disadvantages, depending on the type of neural cells desired. The different methods induce the differentiation of neural tissues with distinct characteristics, particularly with regard to their regional identities in the CNS (2, 5, 8).

We previously reported a feeder cell-dependent induction method that uses a neuralizing activity located on the surface of PA6 stromal cells [stromal cell-derived inducing activity (SDIA)] (6). SDIA induces neural differentiation from mES cells quickly (≤5 days) and efficiently (>90%). In response to exogenous patterning signals such as Sonic hedgehog (Shh), bone morphogenetic protein 4 (BMP4), and RA (8, 10), SDIA-induced neural precursors differentiate into a wide range of neural cells of the CNS that correlate with their positions along the dorsal-ventral and rostral-caudal axes (6, 8). SDIA is also applicable to the generation of medically useful neurons such as dopaminergic neurons and motor neurons not only from mES cells but also from primate ES cells (human and nonhuman) (7, 11, 12). In particular, SDIA-treated ES cells efficiently differentiate into midbrain dopaminergic neurons (≈30% of induced neurons) without the addition of exogenous factors such as Shh (6). This method is in contrast to other methods (e.g., the multiple induction/selection method) (3), which require additional treatment with several inducing factors or gene transfer to efficiently generate dopaminergic neurons. Furthermore, when grafted into the striatum of the 1-methyl-4-phenyl-1,2,3,6-tetrahydropyridine (MPTP)-treated Parkinson's disease model monkey (13), SDIA-induced dopaminergic neurons (from primate ES cells) cause marked improvement in motor function and robustly increase local uptake of the dopamine precursor (Dopa), indicating that the SDIA-induced neurons are functional in the *in vivo* context.

Because of its simple, speedy procedure and good reproducibility, the SDIA method has become one of the standard methods used in human ES (hES) cell-based therapeutic research for neurological diseases such as Parkinson's disease (11, 12, 14–17). However, despite its advantages, the SDIA method has a fundamental practical disadvantage for clinical applications of stem cell therapy: the use of xenogenic (mouse) stromal cells as the source of the inductive signals (6). The involvement of xenogenic cells (and any materials derived from them) presumably increases the risk associated with cocultured tissues in transplantation therapy (18). The hES cell-derived neurons induced with PA6 cells might be contaminated with pathogens or unfavorable antigens originating from the cocultured animal cells. For instance, it has been reported that hES cells cultured on mouse feeder cells express an immunogenic non-human sialic acid on their cell surface (19).

In this study, as an alternative inductive material for neural differentiation of ES cells, we introduce the use of the matrix layers of the human amniotic membrane (hAM). The hAM matrix layers possess intriguing biological activities such as the promotion of wound healing and cell growth (20, 21). Here we show that the hAM matrix layers possess an SDIA-like potent neural-inducing activity. Because the matrix of the hAM is a material widely used in surgical practice (20, 22), it serves as a unique, safe source of neural-inducing factors of human origin, which could circumvent problems associated with the use of xenogenic materials.

Results

Efficient Neural Differentiation of ES Cells on the Denuded hAM. The hAM is composed of an epithelial layer and two matrix layers (the basement membrane and the thick avascular stromal matrix) (23), which underlie the epithelium (illustrated in Fig. 6, which is published as supporting information on the PNAS web site). The matrix layers of hAM (referred to as "denuded hAM"

Conflict of interest statement: No conflicts declared.

This paper was submitted directly (Track II) to the PNAS office.

Abbreviations: mES, mouse ES; hES, human ES; hAM, human amniotic membrane; KSR, knockout serum replacement; AMED, amniotic membrane matrix-based ES cell differentiation; SDIA, stromal cell-derived inducing activity; TH, tyrosine hydroxylase; Shh, Sonic hedgehog; BMP4, bone morphogenetic protein 4; RA, retinoic acid; EB, embryoid bodies.

†Present address: Department of Ophthalmology, National Hospital for Geriatric Medicine, National Center for Geriatrics and Gerontology, Obu 474-8511, Japan.

‖To whom correspondence should be addressed at: Organogenesis and Neurogenesis Group, RIKEN Center for Developmental Biology, 2-2-3 Minatojima-minamimachi, Chuo, Kobe 650-0047, Japan. E-mail: sasaicdb@mub.biglobe.ne.jp.

www.pnas.org/cgi/doi/10.1073/pnas.0600104103

hereafter) have been shown to possess growth-supporting activity on the stem/progenitor cells of various tissues. For instance, corneal limbal progenitors efficiently grow on denuded hAM and eventually form a well organized epithelial tissue, which is suitable for transplantation (21, 22).

We first tested whether the growth of mES cells was supported on the denuded hAM. A detailed protocol is described in the *Supporting Material and Methods*, which is published as supporting information on the PNAS web site, and illustrated in Fig. 1 *A* and *B* and Fig. 6. Dissociated mES cells formed large colonies when cultured for a week on the gelatin-coated denuded hAM in serum-free differentiation medium [knockout serum replacement (KSR)-based or chemically defined medium; see *Materials and Methods*] without leukemia inhibitory factor (Fig. 1*C*, arrow; the porous filter is seen as the background with halos in this picture). These colonies contained a large proportion of Nestin$^+$ and NCAM$^+$ neural cells (>90%; Fig. 1 *D–F*; day 6). We next examined the generation of neural precursors by using an ES cell line in which GFP cDNA was knocked-in at the locus of the early neural gene *Sox1* [*Sox1-GFP*; line 46C; a gift from A. Smith (University of Edinburgh, Edinburgh)] (24). Strong Sox1-GFP expression first appeared in the ES cells between days 3 and 4 (data not shown), and a substantial cell population became Sox1-GFP$^+$ on day 5 and after (≈90% of the cells on day 5; Fig. 1*G*). Most of the Sox1-GFP$^+$ cells (>90%) coexpressed the neural precursor markers Musashi (Fig. 1*H*) and Nestin (data not shown), indicating a preferential generation of neural precursors from ES cells cultured on hAM. In contrast, treatment with BMP4 (0.5 nM, days 0–5), which is a strong inhibitor of early neural differentiation (6), suppressed the Sox1-GFP expression in ES cells cultured on hAM (Fig. 1*I*; instead, the cells expressed the nonneural epithelial marker E-cadherin; see also Fig. 1 *L* and *M*). RT-PCR analysis showed that ES cells cultured on the denuded hAM did not express the mesodermal marker *Brachyury* or the endodermal markers *AFP* and *Sox17* (Fig. 1*J*, lane 3) in contrast to EB treated with serum (lane 2).

The preferential appearance of neural cells in the culture was unlikely to be caused by the selective adhesion of contaminating neural precursors (ES cell-derived) to the hAM for the following reasons. First, the ES cells used in this study expressed Oct3/4 and Nanog (markers of the undifferentiated state; >95%) in the maintenance culture, whereas no Sox1 expression was observed (data not shown). Second, even 1 or 2 days after plating, ES cells growing on the denuded hAM frequently expressed Oct3/4 (>95%) but not Sox1 (Fig. 1*K*), indicating that the attached cells were undifferentiated.

The Sox1-GFP$^+$ cells on the hAM never expressed the human-specific nuclear antigen (25) ($n > 200$ colonies; Fig. 7*A–C*, which is published as supporting information on the PNAS web site), indicating that these cells were not produced by fusion between the mES cells and contaminating human cells on the denuded hAM. Importantly, both the growth-supporting (data not shown) and neural-inducing (Fig. 1 *M* and *N*; shown by the Sox1-GFP$^+$ populations in FACS analyses) activities of the denuded hAM remained unaffected even after treatment with 0.5% deoxycholate (12 h at 37°C), which thoroughly removed the cellular components from the hAM (see *Supporting Materials and Methods*). This finding indicates that the activities are present in the detergent-resistant extracellular matrices.

Taken together, these observations demonstrate that the hAM matrix provides a potent neural-inducing environment for cocultured ES cells. In the present study, "ES cell differentiation on the denuded hAM" is referred to as amniotic membrane matrix-based ES cell differentiation (AMED) hereafter.

On the hAM matrix, as described above, ES cells grew efficiently and selectively differentiated into Sox1$^+$ neural precursors (at a 90% or higher frequency) in serum-free medium. We next examined whether such highly selective, efficient generation of Sox1$^+$ precursors was seen when other matrix materials were used as a substratum. ES cells were cultured on culture dishes coated with gelatin, collagen IV, laminin, or fibronectin or on dishes with a collagen I gel. In all these cases, the cells grew less robustly than on the hAM matrix, and the efficiency of neural differentiation was substantially lower (60–70%; Fig. 7*F*) even though the same serum-free differentiation medium was

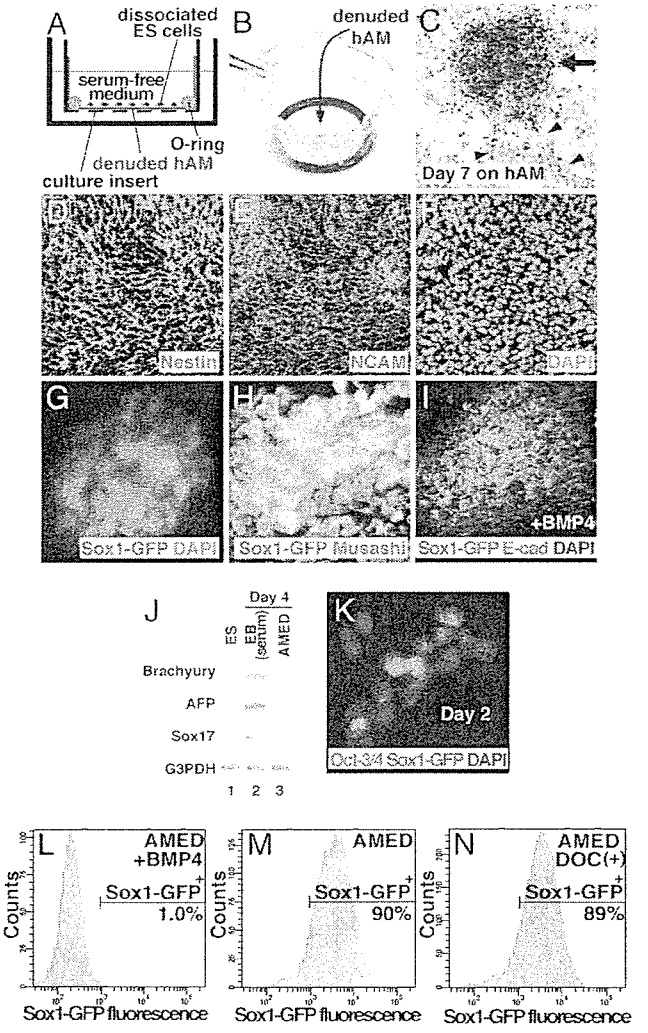

Fig. 1. Efficient induction of neural differentiation from mES cells on the denuded hAM. (*A*) Schematic view of AMED culture. (*B*) Photograph of a culture insert with denuded hAM and O-ring (black). (*C*) Phase-contrast view of a mES cell colony (arrow) cultured on hAM for 1 week. Arrowheads indicate neurites extending from the colony. (*D–F*) Immunostaining of the AMED-treated cells (day 6) with Nestin and NCAM antibodies (*D* and *E*) and nuclear staining with DAPI (*F*). (*G* and *H*) Immunostaining of the AMED-treated cells with neural precursor markers. Sox1-GFP signal (green in *G* and *H*), Musashi (red in *H*, day 7), and DAPI (blue in *G*) are shown. (*I*) Immunostaining analysis of ES cells treated with AMED and BMP4. Sox1-GFP signal (green) was not detected, and most of the cells expressed the nonneural epithelial marker E-cadherin (red), showing that BMP4 inhibited neural differentiation in AMED culture. (*J*) RT-PCR analysis of mesodermal (*Brachyury*) and endodermal (*AFP* and *Sox17*) marker genes. (*K*) Immunostaining of ES cells on hAM for Oct3/4 and Sox1-GFP expression (day 2). Most of the cells expressed Oct3/4 (marker for the undifferentiated state) but not the Sox1-GFP neural precursor marker. (*L–N*) FACS analysis showing efficient neural differentiation (Sox1-GFP expression on day 6) of mES cells cultured on hAM pretreated with deoxycholate (DOC; *N*). (*L*) Negative control for Sox1-GFP expression, ES cells treated with AMED and BMP4 (see also panel *I*). (*M*) Positive control, AMED-treated ES cells.

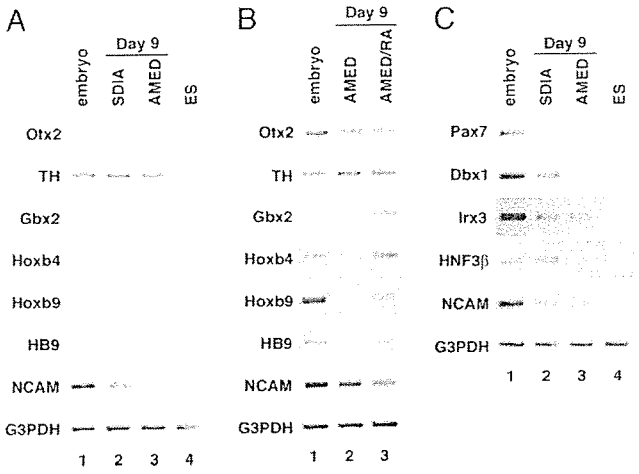

Fig. 2. Regional characterization of AMED-induced neural tissues from mES cells. RT-PCR analysis with the rostral-caudal (*A* and *B*) and dorsal-ventral (*C*) marker genes for CNS tissues. (*A* and *C*) Lane 1, whole embryo (embryonic day 10.5); lane 2, SDIA-treated ES cells (day 9); lane 3, AMED-treated ES cells (day 9); lane 4, undifferentiated ES cells. (*B*) Lane 1, whole embryo (embryonic day 10.5); lane 2, AMED-treated ES cells (day 9); lane 3, AMED- and RA-treated ES cells (day 9).

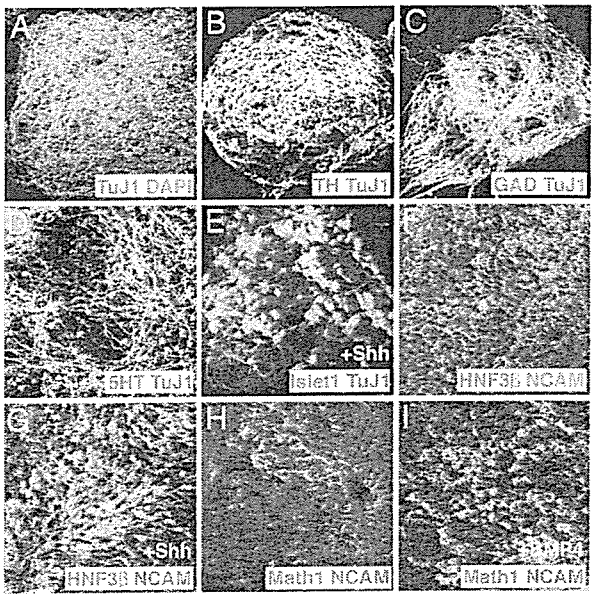

Fig. 3. AMED-treated mES cells generate various types of neural cells including dopaminergic neurons. (*A*) Immunostaining of AMED-treated mES cells with TuJ1 (red) antibody. DAPI, green. (*B–D*) Immunostaining with neurotransmitter-type markers (red) and TuJ1 (green) antibodies (day 13). (*B*) TH for dopamine; (*C*) glutamic acid decarboxylase for GABA; (*D*) 5HT for serotonin. (*E*) Expression of Islet1 in mES cells treated with AMED and Shh (30 nM, days 4–9). (*F* and *G*) Expression of HNF3β in mES cells treated with AMED alone (*F*) and with AMED and Shh (300 nM; *G*). (*H* and *I*) Math1 immunostaining of AMED-treated mES cells with (*I*) or without (*H*) BMP4 treatment (0.5 nM, days 6–10).

used, demonstrating that the hAM matrix has particularly strong supporting activities for the cell growth and neural differentiation of ES cells.

Regional Characterization of the AMED-Induced Neural Tissues. To characterize the nature of the AMED-induced neural tissues, we next performed RT-PCR analyses with regional gene markers. AMED-treated ES cells expressed the forebrain-midbrain markers *Otx2*, *TH* (tyrosine hydroxylase), *Pax2*, and *En2* and the rostral hindbrain marker *Gbx2* at substantial levels (Fig. 2*A*, lane 3 and data not shown). In contrast, little expression was detected for the spinal cord markers *Hoxb4*, *Hoxb9*, and *HB9* (Fig. 2*A*, lane 3).

We recently established another *in vitro* system for neural differentiation of ES cells, namely the SFEB method (serum-free floating culture of EB-like aggregates) (5), which, like AMED, does not use feeder cells as an inducer. SFEB-treated ES cells efficiently generate the rostral-most CNS tissues, particularly Bf1$^+$ telencephalic tissues (15–35%), whereas brainstem tissue differentiation (e.g., dopaminergic neurons) is rare (5). Quantitative analysis using immunostaining indicated that the rostral-most CNS marker Bf1 was rarely expressed in AMED-induced neural cells (<1%; data not shown). Thus, the AMED-induced neural tissues show regional characteristics of the rostral-caudal axis, which are similar to those found in the SDIA culture (mainly brainstem regions) rather than in the SFEB culture (mainly the rostral-most CNS).

The rostral-caudal specification of AMED-induced neural cells could be modified by adding the caudalizing factor RA (Fig. 2*B*). Treatment with RA (0.2 μM, days 4–9) promoted the expression of caudal CNS markers (*Gbx2*, *Hoxb4*, *Hoxb9*, and *HB9*), whereas the forebrain marker *Otx2* was suppressed.

Analyses with dorsal-ventral marker genes showed that the AMED treatment induced both dorsal (*Pax7* and *Dbx1*) and ventral (*Irx3* and *HNF3β*) neural tube markers (Fig. 2*C*, lane 3). Together with the rostral-caudal marker analysis, these findings show that the regional characteristics of the AMED-induced neural tissues are largely similar to those of the SDIA-induced ones (refs. 5 and 8; lane 2 of Fig. 2 *A* and *C*).

AMED-Treated ES Cells Generate a Variety of Neurons Including Dopaminergic Neurons. Immunostaining showed that all of the colonies on day 9 contained a large number of cells that were positive for the postmitotic neuronal marker TuJ1 (62% of total cells; Fig. 3*A*). On day 13, the dopaminergic neuron marker TH was expressed in 39% of the postmitotic neurons (26% of total cells) (Fig. 3*B*). These TH$^+$ neurons were negative for the noradrenergic marker dopamine β-hydroxylase (data not shown). AMED-treated ES cells contained other neuron types as well, such as GABAergic (glutamic acid decarboxylase-positive; 22% of the neurons; Fig. 3*C*) and serotonergic (5HT$^+$; 1–3% of the neurons; typically rostral hindbrain; Fig. 3*D*) neurons.

Neural precursors induced in the AMED culture could respond to embryologically relevant patterning signals. Treatment with the ventralizing factor Shh (30 nM, days 4–9) efficiently induced the expression of the motor neuron marker Islet1 (32% of the neurons; ventral CNS marker; 5% without Shh treatment) in AMED-cultured ES cells (Fig. 3*E* and data not shown). In addition, the differentiation of HNF3β$^+$ NCAM$^+$ cells (floor plate; the ventral-most CNS tissue) was significantly enhanced by Shh treatment at a high dose (3% and 49% of total cells in the absence and presence of 300 nM Shh during days 4–9, respectively; Fig. 3 *F* and *G*). Conversely, treatment with the dorsalizing factor BMP4 (0.5 nM, days 6–10) (8) induced the dorsal CNS marker Math1 (4% of NCAM$^+$ neural cells with BMP4, Fig. 3*I*; <0.1% without BMP4, Fig. 3*H*) but not Islet1 or HNF3β (data not shown).

These observations demonstrate that AMED-induced neural precursors can generate a variety of CNS tissues *in vitro*.

AMED Induces the Differentiation of Neural and Eye Tissues also from hES Cells. Previous studies have shown that the SDIA method is also applicable to neural differentiation of hES cells (11, 12).

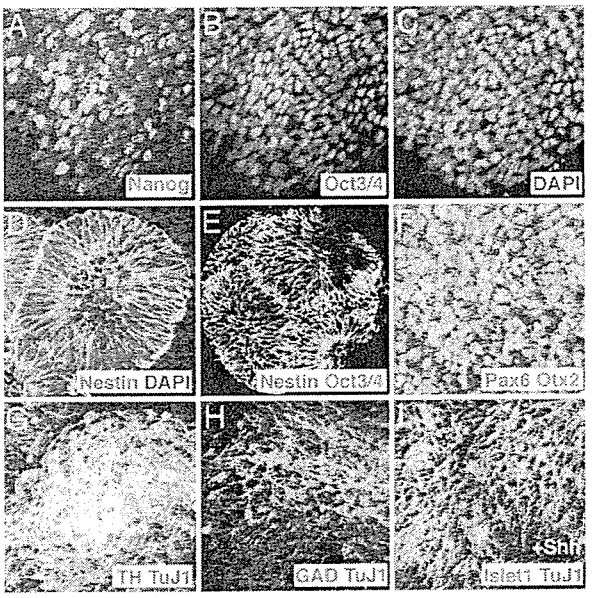

Fig. 4. Neural differentiation of hES cells treated with AMED. (*A–C*) Expression Nanog (red in *A*; Nanog levels were variable as seen in undifferentiated hES cells) and Oct3/4 (green in *B*) in the majority of AMED-treated hES cells on day 2. DAPI (*C*) for nuclear staining. (*D*) Expression of Nestin (green) in AMED-treated hES cells on day 15. DAPI (blue) for nuclear staining. (*E*) Expression of Nestin (green) and Oct3/4 (red) on day 15. (*F*) Mutually exclusive expression of Otx2 (red) and Pax6 (green) in AMED-treated hES cells on day 33. (*G*) Expression of TH (red) in a substantial portion of the TuJ1$^+$ neurons (green) induced from hES cells by AMED (day 40). (*H*) Expression of glutamic acid decarboxylase (red) and TuJ1 (green) on day 42. (*I*) Expression of Islet1 (red) and TuJ1 (green) in AMED/Shh-treated hES cells on day 42.

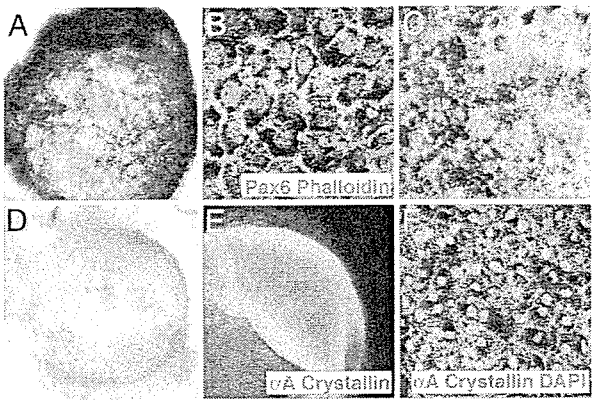

Fig. 5. Differentiation of pigment epithelia and lentoid tissues from AMED-treated hES cells. (*A*) On day 28 and after, pigmented colonies were occasionally found in the culture of hES cells on hAM. (*B*) Phalloidin (red) and anti-Pax6 (green) staining. (*C*) A high-magnification picture of hES cell-derived retinal pigment epithelial cells (pigmented, polygonal) induced in the AMED culture. The pigmented cells were manually isolated from the hAM by a pipette tip and cultured on a culture dish. (*D*) A low-magnification picture of an hES cell-derived lentoid tissue. (*E*) Whole-mount immunostaining with anti-αA-crystallin antibody. (*F*) A high-magnification confocal picture of αA-crystallin (green) and DAPI (red) staining.

Therefore, we next examined whether the AMED treatment promoted neural differentiation also in hES cells. Because hES cells generally do not survive and grow well after complete dissociation, we seeded hES cells in small aggregates (clumps of 5–20 cells) onto the denuded hAM (illustrated in Fig. 8, which is published as supporting information on the PNAS web site). In addition, to enhance cellular attachment to the membrane, the hAM was coated with laminin (see the *Supporting Materials and Methods*). Under these conditions, hES cells reproducibly grew on the hAM and expressed markers for the undifferentiated state (Oct3/4 and Nanog; Fig. 4 *A* and *B*) on day 2. On day 15 of AMED culture, hES cells differentiated into Nestin$^+$ neural precursors at a high frequency (>85% of the cells; Fig. 4*D*). A majority of these Nestin$^+$ neural precursors formed rosette-like clusters. Oct3/4 expression was substantially down-regulated by day 15 and detected only in a small percentage of cells (<5%; they are Nestin$^-$) (Fig. 4*E*; the Oct3/4-positive population disappeared later by day 25). Pax6 expression first appeared on day 15 and was observed in a subpopulation (≈50%) of cells on day 33 (Fig. 4*F*). Expression of the regional marker Otx2 (forebrain and midbrain) was also seen (≈30% of total cells on day 33), whereas the Otx2$^+$ cells were generally negative for Pax6 (Fig. 4*F*). Otx2$^+$/Pax6$^-$ is consistent with the marker expression profile of the midbrain and/or the ventral forebrain, at least in rodent embryos. The telencephalic regional marker Bf1 was not detected in hES cell-derived neural progenitors, at least on and before day 44 (data not shown).

The postmitotic neuronal marker TuJ1 was rarely found on or before day 30 and substantially increased during days 35–40 (Fig. 4*G* and data not shown). On days 40–42, a high percentage of AMED-induced neurons expressed TH (31% of the TuJ1$^+$ neurons; 40% of the total cells were positive for TuJ1; Fig. 4*G*). Expression of the GABAergic neuronal marker glutamic acid decarboxylase was also observed, although less frequently (≈5% of the TuJ1$^+$ neurons; Fig. 4*H*) than TH. The serotonergic neuronal marker (5HT) was detected in <1% neurons (day 44; data not shown). As seen with mES cells (Fig. 3*E*), Shh treatment (300 nM, days 15–42) induced differentiation of Islet1$^+$ neurons in hES cells cultured on the hAM (19% of the TuJ1$^+$ neurons with Shh and <1% without Shh) (Fig. 4*I*).

Our previous studies have shown that SDIA-treated primate ES cells differentiate not only into neural cells but also into eye tissues such as retinal pigment epithelium (7, 26; the retinal pigment epithelium is a CNS tissue derived from the diencephalon during embryogenesis) and lens cells (27). In AMED culture, a number of colonies containing pigmented cells appeared in each well on day 28 (15–40 colonies per well; 200 hES cell clumps were initially seeded per well; Fig. 5*A*). Importantly, these cells were positive for Pax6 and showed actin bundles (Fig. 5*B*; phalloidin staining), consistent with the characteristics of pigment epithelial cells. The pigmented cells could be manually isolated with a pipette tip and grown on a collagen I-coated dish. They exhibited a typical retinal pigment epithelial cell-like morphology (hexagonal cells with a cobblestone-like appearance) (26) under light microscopy (Fig. 5*C*). On day 50 and later, small masses of light-reflecting lentoid tissues were also occasionally found in the culture (Fig. 5*D*). These tissues were αA-crystallin-positive, consistent with the nature of lens cells (Fig. 5 *E* and *F*).

Discussion

Matrix-Associated Neural-Inducing Factors. This study has shown the presence of matrix-associated activities for inducing selective differentiation of neural and sensory tissues from mES and hES cells *in vitro*. Our observations clearly demonstrate that many aspects of the controlled differentiation of AMED-treated ES cells are similar to those of SDIA-treated ones (6–8, 26, 27). Thus, the hAM matrix provides a reasonable human-derived candidate material that can substitute for the mouse-derived feeder layer of PA6 cells as a unique, versatile inducer for neural differentiation in ES cell culture.

At the present, the molecular nature of the inducing activity on the hAM matrix remains to be identified, as does that of the activity on the PA6 cells. A particularly intriguing subject for

DEVELOPMENTAL BIOLOGY

future study is to determine how several activities common to the AMED and SDIA methods (e.g., growth support, induction of neural precursors, and differentiation of dopaminergic neurons) are related at the molecular level.

Another important issue, from the mechanistic viewpoint, is to learn which cells are responsible for the accumulation of the AMED activity on the hAM matrix. In the light of their anatomical relationship, one obvious candidate is the amniotic epithelium, which overlies the hAM matrix layers. However, in a preliminary study, we found that neither the amniotic epithelial cells nor their pericellular matrix promotes neural differentiation of cocultured ES cells (our unpublished observations), indicating that the amniotic epithelium, at least by itself, is unlikely to explain the production of the AMED activity.

AMED Culture as a Versatile Method for Generating Neural Cells. The AMED system has several advantages for use in ES cell-based regenerative medicine. (*i*) The AMED culture is remarkably simple; ES cells are plated on the denuded hAM and cultured in a simple serum-free medium. (*ii*) The AMED method uses a human-derived material (denuded hAM) for which the biological safety has been demonstrated for decades in the clinical practices of dermatology and ophthalmology (20, 28, 29). (*iii*) hAM is routinely obtainable from Caesarian sections with proper informed consents. (*iv*) hAM can be easily stored at −80°C for at least for 6 months without losing its AMED activity (see *Supporting Materials and Methods*). Moreover, the neural-inducing activity on the denuded hAM is retained even after lyophilization/rehydration (Fig. 7*G*; lyophilization followed by vacuum packaging and γ-ray irradiation and rehydration in culture medium for 1 hour before use) (30). Therefore, the AMED method could be used to prepare ES cell-derived neurons for cell therapy, regardless of the distance between stem cell laboratories and obstetric clinics.

In future technical improvements of the AMED method, solubilization of the AMED activity from the hAM matrix may be useful because a soluble matrix material could be used to coat culture dishes or even three-dimensional polymer scaffolds (which can support tissue formation from RA-induced neural tissues from hES cells; ref. 31) to further simplify the AMED procedure.

In conclusion, this study demonstrates that the AMED method is potentially useful for producing various neurons for cell therapy from ES cells and that AMED provides a practical solution to avoid the use of xenogenic materials, which are used in the SDIA method.

Materials and Methods

ES Cell Culture. For the maintenance (6), undifferentiated mES cells (EB5 and 46C) were cultured on gelatin-coated dishes at 37°C under 5% CO_2 in Glasgow-MEM (Invitrogen) supplemented with 1% FCS (JRH Biosciences, Lenexa, KS), 10% KSR (Invitrogen), 2 mM glutamine, 0.1 mM nonessential amino acids, 1 mM pyruvate, 0.1 mM 2-mercaptoethanol, and 2,000 units/ml leukemia inhibitory factor (Invitrogen). PA6 cells were maintained in α-MEM with 10% FCS (HyClone) (32).

The hES cells (KhES-1) were a gift from N. Nakatsuji and H. Suemori (Kyoto University) and were used following the hES cell guidelines of the Japanese government. Undifferentiated hES cells were maintained on a feeder layer of mouse embryonic fibroblasts (Invitrogen; inactivated with 10 μg/ml mitomycin C) in DMEM/F12 (Sigma) supplemented with 20% KSR, 2 mM glutamine, 0.1 mM nonessential amino acids (Invitrogen), 5 ng/ml recombinant human bFGF (Upstate), and 0.1 mM 2-mercaptoethanol under 2% CO_2. For passaging, hES cell colonies were detached and recovered *en bloc* from the feeder layer by treating them with 0.25% trypsin and 0.1 mg/ml collagenase IV in PBS containing 20% KSR and 1 mM $CaCl_2$ at 37°C for 7 min, followed by tapping the cultures and flushing them with a pipette. After two volumes of culture medium was added, the detached ES cell clumps were broken into smaller pieces (5–20 cells) by gently pipetting several times. The passages were performed at a 1:4 split ratio. For storage, the ES cell colonies were recovered *en bloc* (without further dissociation) from a 6-cm culture dish, suspended in 1 ml of ice-cold culture medium supplemented with 2 M DMSO, 1 M acetamide, and 3 M polypropylene glycol, and quickly frozen in a 2-ml cryogenic tube (Becton Dickinson Labware) by directly submerging the tube in liquid N_2. The day on which ES cells were seeded on hAM or PA6 cells to start differentiation was defined as day 0.

Preparation of Denuded hAM. With proper informed consent following the tenets of the Declaration of Helsinki, human AMs were obtained under aseptic conditions at the time of Caesarean section. The method of removing the amniotic epithelium from the amniotic membrane has been reported (refs. 21 and 22; see also *Supporting Materials and Methods*). The experiments using the hAM were performed according to the institutional guidelines for human-derived materials.

AMED Culture. The detailed procedures of the AMED culture with mES and hES cells are illustrated in Figs. 6 and 8 and described in the *Supporting Materials and Methods*. For the differentiation medium in this study, we used the KSR-containing G-MEM medium, which was also used in the previous SDIA experiments (6): G-MEM supplemented with 10% KSR, 2 mM glutamine, 1 mM pyruvate, 0.1 mM nonessential amino acids, 0.1 mM 2-mercaptoethanol, 100 units/ml penicillin, and 100 μg/ml streptomycin. In addition to the KSR-based medium used here, we found that chemically defined medium (which does not contain KSR) (33) was suitable for promoting neural differentiation in the AMED culture. The formulation of chemically defined medium is as follows: Iscove's modified Dulbecco's medium/Ham's medium F12 (1:1 ratio) supplemented with glutamine as L-alanyl-L-glutamine or GlutaMAX-I (2 mM; Invitrogen), 5 mg/ml BSA (fraction V), 1× chemically defined lipid concentrate (Invitrogen), 15 μg/ml human apo-transferrin, 0.45 mM monothioglycerol, 7 μg/ml insulin, and 1 unit/ml leukemia inhibitory factor.

Immunostaining, RT-PCR, and FACS Analyses. The antibodies used for immunostaining are listed in the *Supporting Materials and Methods*. Cells were fixed with 4% paraformaldehyde at 4°C for 15 min, and immunostaining was performed as described in refs. 5 and 8 and using secondary antibodies conjugated with FITC, cy3, or cy5. For immunostaining cells in large colonies, confocal microscopy (LSM 510; Zeiss) was used to observe the cells inside the colony with good resolution. The total number of cells was counted by staining nuclei with DAPI. For statistical analyses, 100–200 colonies were examined in each experiment. Experiments were performed at least three times. The values shown in the graphs represent the mean ± SD. RT-PCR was performed with ES cell colonies mechanically detached from the hAM or enzymatically detached from feeder cells as described in refs. 8 and 10. FACS analysis using ES cells with the Sox1-GFP reporter was performed as described in refs. 5 and 24.

We thank H. Niwa (RIKEN Center for Developmental Biology) for the EB5 cells and helpful comments on this work, A. Smith (University of Edinburgh) for the Sox1-GFP ES cells, H. Suemori and N. Nakatsuji (Kyoto University) for providing the hES cell line, H. Kitajima in the Niwa laboratory for kind advice on hES cell expansion and storage, and to the members of the Sasai laboratory for stimulating discussion. This work was supported by grants-in-aid from the Ministry of Education, Culture, Sports, Science, and Technology of Japan (to S.K. and Y.S.), the Kobe Cluster Project (to S.K. and Y.S.), and the Leading Project (to Y.S. and M.T.).

1. Bain, G., Kitchens, D., Yao, M., Huettner, J. E. & Gottlieb, D. I. (1995) *Dev. Biol.* **168,** 342–357.
2. Wichterle, H., Lieberam, I., Porter, J. A. & Jessell, T. M. (2002) *Cell* **110,** 385–397.
3. Lee, S.-H., Lumelsky, N., Studer, L., Auerbach, J. M. & McKay, R. D. (2000) *Nat. Biotechnol.* **18,** 675–679.
4. Ying, Q.-L., Stavridis, M., Griffiths, D., Li, M. & Smith, A. (2003) *Nat. Biotechnol.* **21,** 183–186.
5. Watanabe, K., Kamiya, D., Nishiyama, A., Katayama, T., Nozaki, S., Kawasaki, H., Watanabe, Y., Mizuseki, K. & Sasai, Y. (2005) *Nat. Neurosci.* **8,** 288–296.
6. Kawasaki, H., Mizuseki, K., Nishikawa, S., Kaneko, S., Kuwana, Y., Nakanishi, S., Nishikawa, S.-I. & Sasai, Y. (2000) *Neuron* **28,** 31–40.
7. Kawasaki, H., Suemori, H., Mizuseki, K., Watanabe, K., Urano, F., Ichinose, H., Haruta, M., Takahashi, M., Yoshikawa, K., Nishikawa, S.-I., *et al.* (2002) *Proc. Natl. Acad. Sci. USA* **99,** 1580–1585.
8. Mizuseki, K., Sakamoto, T., Watanabe, K., Muguruma, K., Ikeya, M., Nishiyama, A., Arakawa, A., Suemori, H., Nakatsuji, N., Kawasaki, H., *et al.* (2003) *Proc. Natl. Acad. Sci. USA* **100,** 5828–5833.
9. Barberi, T., Klivenyi, P., Calingasan, N. Y., Lee, H., Kawamata, H., Loonam, K., Perrier, A. L., Bruses, J., Rubio, M. E., Topf, N., *et al.* (2003) *Nat. Biotechnol.* **21,** 1200–1207.
10. Irioka, T., Watanabe, K., Mizusawa, H., Mizuseki, K. & Sasai, Y. (2005) *Dev. Brain. Res.* **154,** 63–70.
11. Buytaert-Hoefen, K. A., Alvarez, E. & Freed, C. R. (2004) *Stem Cells* **22,** 669–674.
12. Brederlau, A., Correia, A. S., Anisimov, S. V., Elmi, M., Roybon, L., Paul, G., Morizane, A., Bergquist, F., Riebe, I., Nannmark, U., *et al.* (2006) *Stem Cells,* in press.
13. Takagi, Y., Takahashi, J., Saiki, H., Morizane, A., Hayashi, T., Kishi, Y., Fukuda, H., Okamoto, Y., Koyanagi, M., Ideguchi, M., Hayashi, H., *et al.* (2005) *J. Clin. Invest.* **115,** 102–109.
14. Zeng, X., Chen, J., Liu, Y., Luo, Y., Schulz, T. C., Robins, A. J., Rao, M. S. & Freed, W. J. (2004) *Restor. Neurol. Neurosci.* **22,** 421–428.
15. Zeng, X., Cai, J., Chen, J., Luo, Y., You, Z.-B., Fotter, E., Wang, Y., Harvey, B., Miura, T., Backman, C., *et al.* (2004) *Stem Cells* **22,** 925–940.
16. Pomp, O., Brokhman, I., Ben-Dor, I., Reubinoff, B. & Goldstein, R. S. (2005) *Stem Cells* **23,** 923–930.
17. Goldman, S. (2005) *Nat. Biotechnol.* **23,** 862–871.
18. Takeuchi, Y., Magre, S. & Patience, C. (2005) *Rev. Sci. Tech.* **24,** 323–334.
19. Martin, M. J., Muotri, A., Gage, F. & Varki, A. (2005) *Nat. Med.* **11,** 228–232.
20. Trelford, J. D. & Trelford-Sauder, M. (1979) *Am. J. Obstet. Gynecol.* **134,** 833–845.
21. Koizumi, N., Fullwood, N. J., Bairaktaris, G., Inatomi, T., Kinoshita, S. & Quantock, A. J. (2000) *Invest. Ophthalmol. Visual Sci.* **41,** 2506–2513.
22. Koizumi, N., Inatomi, T., Suzuki, T., Sotozono, C. & Kinoshita, S. (2001) *Ophthalmology* **108,** 1569–1574.
23. Bourne, G. L. (1960) *Am. J. Obstet. Gynecol.* **79,** 1070–1073.
24. Aubert, J., Stavridis, M. P., Tweedie, S., O'Reilly, M., Vierlinger, K., Li, M., Ghazal, P., Pratt, T., Mason, J. O., Roy, D., *et al.* (2003) *Proc. Natl. Acad. Sci. USA* **100,** 11836–11841.
25. Uchida, N., Buck, D. W., He, D., Reitsma, M. J., Masek, M., Phan, T. V., Tsukamoto, A. S., Gage, F. H. & Weissman, I. L. (2000) *Proc. Natl. Acad. Sci. USA* **97,** 14720–14725.
26. Haruta, M., Sasai, Y., Kawasaki, H., Amemiya, K., Ooto, S., Kitada, M., Suemori, H., Nakatsuji, N., Ide, C., Honda, Y., *et al.* (2004) *Invest. Ophthalmol. Visual Sci.* **45,** 1020–1025.
27. Ooto, S., Haruta, M., Honda, Y., Kawasaki, H., Sasai, Y. & Takahashi, M. (2003) *Invest. Ophthalmol. Visual Sci.* **44,** 2689–2693.
28. Tsubota, K., Satake, Y., Ohyama, M., Toda, I., Takano, Y., Ono, M., Shinozaki, N. & Shimazaki, J. (1996) *Am. J. Ophthalmol.* **122,** 38–52.
29. Lee, S.-H. & Tseng, S. C. G. (1997) *Am. J. Ophthalmol.* **123,** 303–312.
30. Nakamura, T., Yoshitani, M., Rigby, H., Fullwood, N. J., Ito, W., Inatomi, T., Sotozono, C., Nakamura, T., Shimizu, Y. & Kinoshita, S. (2004) *Invest. Ophthalmol. Visual Sci.* **45,** 93–99.
31. Levenberg, S., Huang, N. F., Lavik, E., Rogers, A. B., Itskovitz-Eldor, J., Langer, R. (2003) *Proc. Natl. Acad. Sci. USA* **100,** 12741–12746.
32. Kawasaki, H., Mizuseki, K. & Sasai, Y. (2001) in *Methods in Molecular Biology* **185,** ed. Turksen, K. (Humana, Totowa, NJ), pp. 217–227.
33. Johansson, B. M. & Wiles, M. V. (1995) *Mol. Cell. Biol.* **15,** 141–151.

Available online at www.sciencedirect.com
SCIENCE DIRECT®
Experimental Eye Research xx (2006) 1–6
EXPERIMENTAL EYE RESEARCH
www.elsevier.com/locate/yexer

Different expression of angiogenesis-related factors between human cultivated corneal and oral epithelial sheets

Eiichi Sekiyama [a,*], Takahiro Nakamura [a,b], Satoshi Kawasaki [a], Hisayo Sogabe [a], Shigeru Kinoshita [a]

[a] *Department of Ophthalmology, Kyoto Prefectural University of Medicine, Graduate School of Medicine, Kawaramachi Hirokoji, Kamigyo-ku, Kyoto 602-0841, Japan*
[b] *Research Center for Regenerative Medicine, Doshisha University, Kyoto, Japan*

Received 15 August 2005; accepted in revised form 25 February 2006

Abstract

We developed a cultivated oral mucosal epithelial sheet (COE) transplantation system to address severe human ocular surface disorders. Unlike the cultivated corneal epithelial sheet (CCE), the COE induces mild superficial peripheral neovascularization although central clarity is maintained. To evaluate the characteristic differences between CCE and COE regarding to angiogenesis, we examined the expression of angiogenesis-related factors in CCE and COE. Using samples of CCE and COE, we immunohistochemically determined protein expression of the angiogenesis related factors: Thrombospondin-1 (TSP-1), pigment epithelium derived factor (PEDF), endostatin, angiostatin, vascular endothelial growth factor (VEGF), Fms-like tyrosine kinase 1 (Flt-1), kinase insert domain receptor (KDR), and basic fibroblast growth factor (bFGF). We used Western blot analysis to confirm the factors that were immunohistochemically different in CCE and COE. The immunohistochemical staining intensity of TSP-1 was higher in CCE than COE and by Western blot analysis the expression of TSP-1 was significantly higher in CCE than COE ($P < 0.05$). PEDF and endostatin stained moderately stronger in CCE than COE. Immunohistochemically there was no obvious difference between CCE and COE with respect to angiostatin, VEGF, Flt-1, KDR, and bFGF. In comparison with CCE, COE showed decreased expression of anti-angiogenic factors particularly TSP-1. This different expression may relate to the superficial peripheral neovascularization encountered after COE transplantation.

Keywords: cultivated epithelial sheet; angiogenesis; thrombospondin-1; ocular surface reconstruction

1. Introduction

To repair severe ocular surface disorders induced by chemical and thermal injuries, Stevens–Johnson syndrome, and ocular cicatricial pemphigoid, we developed a corneolimbal epithelial culture system that uses amniotic membrane (AM) as a carrier (Koizumi et al., 2000a, 2001) and succeeded in the transplantation of cultivated corneal epithelial sheets (CCE). We chose oral mucosa as a source of epithelial cells (Gipson et al., 1986) to establish an autologous transplantation system. We then developed a method for oral epithelial cell cultivation, and succeeded in the transplantation of cultivated oral epithelial sheets (COE) (Nakamura et al., 2004a,b).

Although COE and CCE share many histological (Fig. 1A1–4) and immunohistochemical characteristics and transmission electron microscopy failed to detect marked differences (Nakamura et al., 2004b), the clinical course of patients who received autologous COE transplants differs from that of CCE recipients. Unlike patients transplanted with CCE, most recipients of autologous COE, irrespective of diseases, developed superficial corneal neovascularization measuring 3–4 mm in length from the limbus under the transplanted epithelial sheet (Nakamura et al., 2004b; Nishida

* Corresponding author. Tel.: +81 75 251 5578; fax: +81 75 251 5663.
E-mail address: esekiyam@ophth.kpu-m.ac.jp (E. Sekiyama).

0014-4835/$ - see front matter © 2006 Elsevier Ltd. All rights reserved.
doi:10.1016/j.exer.2006.02.015

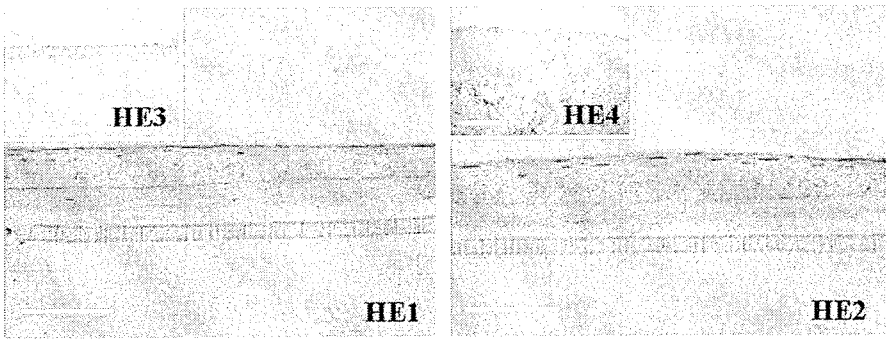

Fig. 1. Representative hematoxylin-eosin staining for CCE (HE1), COE (HE2), normal corneal epithelium (HE3) and normal oral epithelium (HE4).

et al., 2004). Little is known about the pathogenesis of neovascularization after COE transplantation.

We postulated that the mechanism(s) underlying the observed neovascularization was attributable to some characteristics of the oral epithelial cells, and compared CCE and COE with respect to the expression of major angiogenesis-related factors. As our early comparison of the comprehensive gene expression patterns of angiogenesis-related factors in the human corneal- and conjunctival epithelium had shown that only thrombospondin-1 (TSP-1) was significantly up-regulated in the corneal epithelium (Sekiyama et al., 2006), we focused on several factors expressed in the corneal epithelium, including TSP-1. Here we report our first attempt to understand the mechanism(s) of neovascularization after COE transplantation.

2. Materials and methods

2.1. Cultivation of human corneal and oral epithelial cells

Human corneal and oral epithelium, and AM were obtained from donors who provided prior informed consent. Our study followed the tenets of the Declaration of Helsinki and was approved by the Institutional Review Board of Kyoto Prefectural University of Medicine. For epithelial cell culture, five human corneal tissues were obtained from a United States eye bank and five oral mucosal biopsy specimens were donated by healthy volunteers.

For the preparation of human CCE and COE we used a previously reported method (Koizumi et al., 2000b; Nakamura et al., 2003) in which epithelial cells are co-cultured with mitomycin C-inactivated 3T3 fibroblasts. Denuded AM was spread, epithelial basement membrane side up, on the bottom of culture plate inserts (Corning Inc., Corning, NY) and these were placed in dishes containing treated 3T3 fibroblasts. Enzymatically treated corneal limbal or oral epithelial cells were seeded onto the denuded AM prior to 1–2-week submersion in medium. This was followed by 2–3-day exposure to air by lowering the level of the medium (airlifting) to promote epithelial differentiation and barrier function (Koizumi et al., 2000b).

For the controls we used normal human corneal epithelium from corneal buttons of patients undergoing PKP surgery for mild Fuchs corneal dystrophy and superfluous oral tissues from patients who had undergone oral surgery.

2.2. Immunohistochemistry for angiogenesis-related factors

We immunohistochemically investigated the anti-angiogenic factors thrombospondin-1 (TSP-1), pigment epithelium derived factor (PEDF), endostatin, and angiostatin, and the angiogenic factors vascular endothelial growth factor (VEGF), Fms-like tyrosine kinase 1 (Flt-1), kinase insert domain receptor (KDR), and basic fibroblast growth factor (bFGF) in CCE and COE using a modification of our previously described method (Nakamura et al., 2003). Normal human corneal- and oral epithelia were examined for comparison purposes. Briefly, semi-thin (8 μm) cryostat sections were cut from unfixed tissue embedded in optimal cutting temperature compound (Tissue-Tek; Miles Inc., Elkhart, IN). After 5-min fixation in cold acetone the sections were incubated for 15 min with 10% goat serum and 1% bovine serum albumin (Sigma, St. Louis, MO). Then they were incubated at room temperature (RT) for 1 h with the primary antibodies (Table 1) and washed three times for 10 min each in phosphate-buffered saline (PBS). In control experiments we replaced the primary antibody with identical concentrations of the appropriate non-specific normal mouse and rabbit IgG (Dako, Kyoto, Japan). In the negative controls we replaced the primary antibody with the appropriate non-immune IgG.

After incubation with the primary antibody, the sections were washed with PBS containing 0.15% TritonX-100 (PBST) and incubated for 1 h at RT with the appropriate

Table 1
Primary antibodies used for immunohistochemistry

Antibodies	Category	Dilution	Source
TSP-1	Mouse monoclonal	×100	Sigma (St. Louis, MO)
PEDF	Mouse monoclonal	×100	Chemicon (Temecula, CA)
Endostatin	Mouse monoclonal	×100	Upstate (Lake Placid, NY)
Angiostatin	Rabbit monoclonal	×50	Oncogene (San Diego, CA)
VEGF	Mouse monoclonal	×100	Upstate (Lake Placid, NY)
Flt-1	Mouse monoclonal	×30	Chemicon (Temecula, CA)
KDR	Mouse monoclonal	×40	Abcam (Cambridge, MA)
bFGF	Mouse monoclonal	×100	Upstate (Lake Placid, NY)

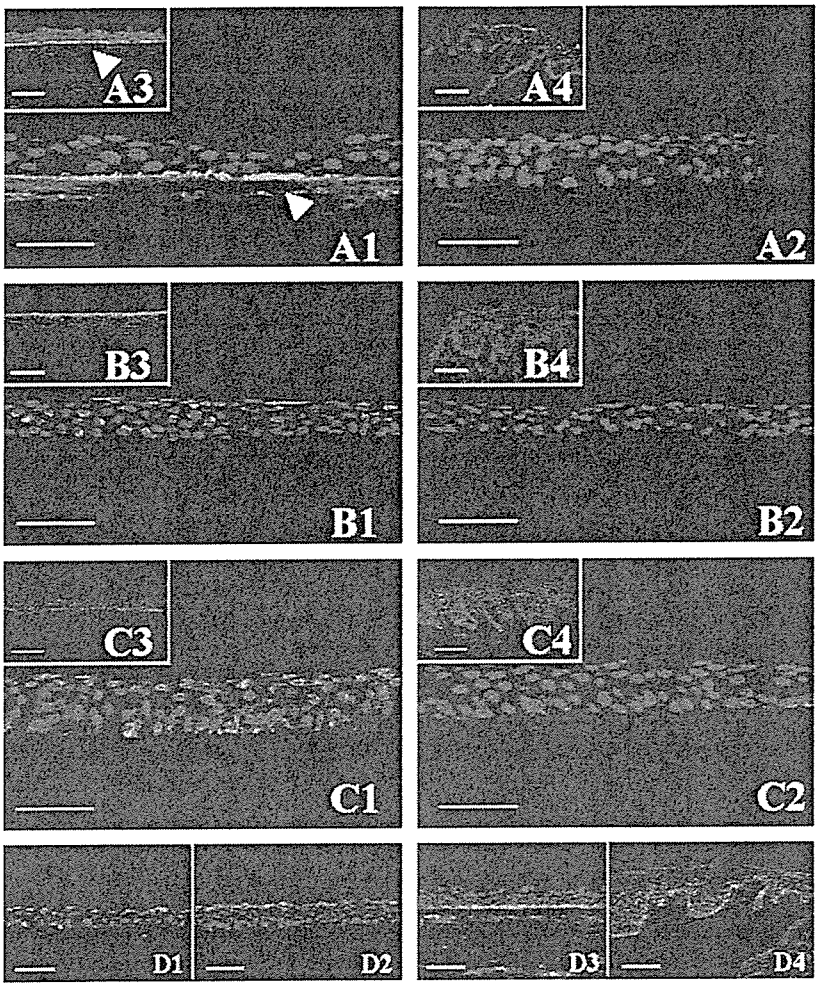

Fig. 2. Representative immunohistochemical staining for anti-angiogenic factors TSP-1 (A), PEDF (B), endostatin (C) and angiostatin (D) in CCE (1), COE (2), normal corneal epithelium (3) and normal oral epithelium (4). TSP-1 was expressed in the basal layer of CCE (A1, arrow) and normal corneal epithelium (A3, arrow), and much less strongly in COE (A2) and normal oral epithelium (A4). PEDF was expressed slightly in CCE (B1), barely in COE (B2), and in the superficial and middle layer of normal corneal epithelium (B3). It was not expressed in normal oral epithelium (B4). Endostatin was expressed in CCE (C1) and normal corneal epithelium (C3), and barely expressed in COE (C2) and normal oral epithelium (C4). Angiostatin was expressed in all examined epithelia (D1–4). Scale bars: 1 and 2: 50 μm; 3: 100 μm; 4: 200 μm.

secondary antibodies, FITC-conjugated anti-mouse, or rabbit IgG antibodies (Molecular Probes Inc., Eugene, OR). After several washes with PBS, the sections were coverslipped using antifade mounting medium containing propidium iodide (Vectashield; Vector, Burlingame, CA) and examined under a confocal microscope (Fluoview; Olympus, Tokyo, Japan).

2.3. Western blot analysis

In our immunohistochemical studies, each fluorescent image was qualitatively and independently scored (3: intense; 2: moderate; 1: faint; 0: negligible) by four examiners in a masked fashion. We took the average of the points scored by the examiners for each sample and assessed statistical significance with the Mann–Whitney *U*-test. Since there was a significant difference between the scores assigned for CCE and COE, we performed Western blots for TSP-1 analysis. CCE and COE were lysed with PBS with 0.1% SDS and 0.1% Triton. For the positive control we used normal human corneal epithelium. The protein content of lysates was determined by bicinchoninic acid (BCA) protein assay (Pierce, Rockford, IL). Aliquots of the lysates were diluted 1:1 with sample buffer (Owl Scientific Inc., Woburn, MA) and heated for 5 min at 95 °C. Equal quantities of protein from lysates (10 μg in 12.5% gel) were subjected to 1 h SDS–PAGE at RT. The separated proteins were then transferred to polyvinylidene difluoride membranes (Immuno-Blot™ PVDF Membrane; Bio-Rad, Hercules, CA) for 12 h at 4 °C and after transfer, the blots were incubated for 30 min in blocking solution (Perfect-Block, MoBi Tec, Goettingen, Germany), washed three times for 10 min each with washing buffer (Tris-buffered saline with 0.1% Tween-20) and then probed for 1 h with anti-TSP-1 (Santa Cruz Biotechnology, Santa Cruz, CA) diluted with washing buffer. After

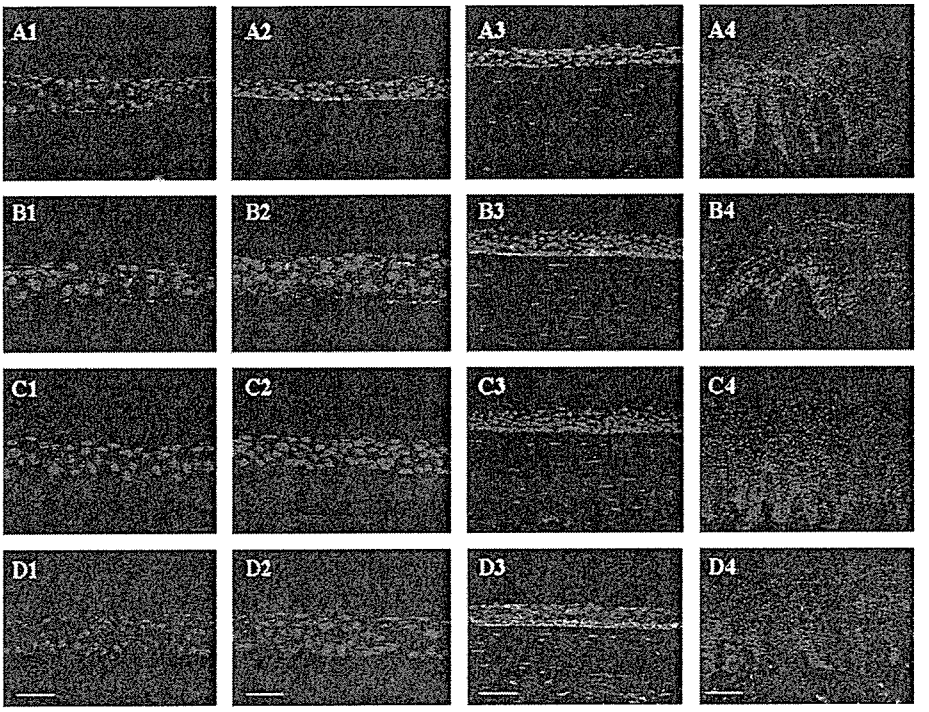

Fig. 3. Representative immunohistochemical staining for angiogenic factors VEGF (A), Flt-1 (B), KDR (C), bFGF (D) in CCE (1), COE (2), normal corneal epithelium (3) and normal oral epithelium (4). VEGF was expressed in the entire layer of CCE (A1), and COE (A2), in the entire, especially the superficial, layer of normal corneal epithelium (A3), and in the middle layer of normal oral epithelium (A4). Flt-1 was weakly expressed in all examined epithelia (B1–4). KDR was not expressed in any examined epithelia (C1–4). Basic FGF was not expressed in CCE and COE (D1 and 2) but was expressed in the basal layer of normal corneal epithelium (D3, arrow) and the middle layer of normal oral epithelium (D4). Scale bars: 1 and 2: 50 μm; 3: 100 μm; 4: 200 μm.

incubation with the primary antibody, the blots were washed three times for 10 min each with washing buffer and then probed with the biotinylated alkaline phosphatase-conjugated secondary antibody (Bio-Rad) diluted with washing buffer. The blots were subsequently developed using the Immune-Blot detection kit (Bio-Rad) and the membranes were then scanned into a computer where band density was digitized using NIH image software.

3. Results

3.1. Immunohistochemistry of human corneal and oral epithelial culture sheets

Cryopreserved CCE and COE were examined. Negative-control sections, incubated with normal mouse and rabbit IgG in the absence of primary antibody, exhibited no discernible specific immunoreactivity over the entire region.

While we detected TSP-1 beneath the cultivated corneal epithelial cells (Fig. 2A1) and normal corneal epithelium (Fig. 2A3), its expression in COE (Fig. 2A2) and normal oral epithelium was minimal or absent (Fig. 2A4). PEDF, slightly expressed in CCE (Fig. 2B1) and barely expressed in COE (Fig. 2B2), was expressed in the superficial and middle layer of normal corneal epithelium (Fig. 2B3) but not in normal oral epithelium (Fig. 2B4). Endostatin, expressed in the entire layer of CCE (Fig. 2C1), in normal corneal epithelium (Fig. 2C3), and in the middle layer of normal oral epithelium (Fig. 2C4), was not expressed in COE (Fig. 2C2). There was no obvious difference between CCE and COE in the expression of angiostatin (Fig. 2D1–4). The staining intensity for TSP-1 was clearly higher in CCE than COE and the staining intensity for PEDF and endostatin was moderately higher in CCE than COE.

VEGF and Flt-1 were expressed in all epithelia examined and there was no significant difference between CCE and COE (Fig. 3A1–4 and B1–4). None of the examined epithelia expressed KDR (Fig. 3C1–4). Basic FGF was not expressed in CCE or COE, but was expressed in the basal layer of normal corneal epithelium and in the middle layer of normal oral epithelium (Fig. 3D1–4). A summary of our immunohistochemical results is provided in Table 2.

3.2. Western blot analysis for TSP-1

We performed Western blots for TSP-1 to determine the protein expression level in CCE and COE. In the presence of TSP-1 antibody there clearly was a single protein band (Fig. 4A); its density was analyzed with NIH image software. As shown in Fig. 4B, TSP-1 was expressed more highly in CCE than COE ($P < 0.05$ by the Mann–Whitney U-test).

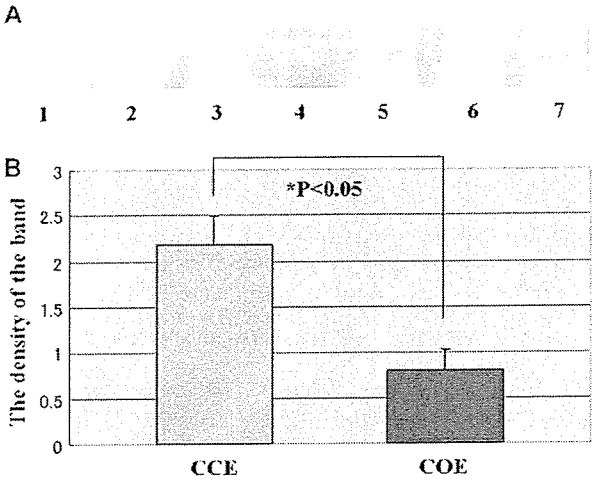

Fig. 4. (A) For TSP-1, Western blots of extracts from CCE (lanes 1, 2, 3) and COE (lanes 5, 6, 7) are shown. Lane 4 shows the molecular weight marker (150 kDa). (B) Average band density analyzed with NIH image software. The density of the CCE is significantly higher than in the COE ($P < 0.05$). The results were statistically compared using the Mann–Whitney U-test. ($n = 3$; mean ± SD: 0.12, mean ± SD: 0.09).

4. Discussion

Immunohistochemically, the staining intensity for TSP-1, the major anti-angiogenic factor contributing to corneal avascularity (Tuszynski and Nicosia, 1996; Castle et al., 1997; Iruela-Arispe et al., 1999; Cursiefen et al., 2004), was higher in CCE than COE and although Western blot analysis detected TSP-1 in both CCE and COE, it was more highly expressed in CCE ($P < 0.05$). Previous studies in TSP-1 knockout mice revealed that their sutured corneas exhibited significantly higher angiogenesis compared with the background strains (Cursiefen et al., 2004). This observation led to the suggestion that TSP-1 plays a role in the suppression of inflammation-induced corneal angiogenesis and that the corneal angiogenic privilege is actively maintained. As the neovascularization we observed in the human recipients of COE transplants may be comparable to the suture-induced angiogenesis in mice, we suggest that the murine findings support our hypothesis that the inflammation-induced corneal neovascularization in the recipients of COE is attributable to the low expression of TSP-1 in these tissues.

Table 2
Immunohistochemical results for each angiogenic factor in each of the examined samples

Factor	NCE	NOE	CCE	COE
TSP-1	2+	0.5+	2+	0.5+
PEDF	2+	–	+	–
Endostatin	+	0.5+	+	–
Angiostatin	+	+	+	+
VEGF	+	+	+	+
Flt-1	+	+	+	+
KDR	–	–	–	–
bFGF	+	+	–	–

NCE, normal corneal epithelium; NOE, normal oral epithelium. 2+, intense expression; +, moderate expression; 0.5+, faint expression; –, negligible expression. Staining intensities for TSP-1, PEDF and endostatin were higher in CCE than COE, and the intensity of TSP-1 staining was particularly high in CCE.

Immunohistochemistry detected TSP-1 expression not only beneath the basal epithelial cells of CCE, but also in AM (Fig. 1B3). As TSP-1 is secreted by fibroblasts, vascular endothelial cells, and smooth muscle cells (Mumby et al., 1984), the TSP-1 we detected could have been secreted by fibroblasts in the stroma of AM. To rule out the possibility that the different expression of TSP-1 in CCE and COE was due to variations in the AM, we performed identical experiments using γ-ray-sterilized AM (Nakamura et al., 2004c) which rendered the fibroblasts not viable. As was the case in denuded AM, TSP-1 was expressed beneath the basal epithelial cells of CCE grown on sterilized AM (data not shown). This observation confirms that the TSP-1 we observed was secreted not by fibroblasts in the stroma of AM, but by epithelial cells, particularly corneal epithelial cells.

Immunohistochemically, the staining intensity for PEDF was slightly higher in CCE than COE. Although we did not perform quantitative PEDF analysis here, studies are underway to examine whether PEDF is an inhibitor of neovascularization under COE. PEDF is one of the major anti-angiogenic factors essential for corneal avascularity (Murthy et al., 2003; Shao et al., 2004) and it more effectively inhibits endothelial cell migration than TSP-1, endostatin, and angiostatin (Dawson et al., 1999).

Endostatin, a potent angiogenesis inhibitor and contributor to corneal avascularity (Chang et al., 2001; Lin et al., 2001; Morbidelli et al., 2003), is expressed in CCE, but not in COE. We are in the process of examining the possible inhibitory effects of endostatin on neovascularization under COE. Ma et al. (2004), who examined the in vitro anti-angiogenic activities of human corneal epithelial cells cultivated on human AM, found that endostatin was a major factor contributing to the anti-angiogenic activity exhibited by human corneal limbal epithelial cells. When they quantitated anti-angiogenic factors in culture supernatants, they found that only the endostatin level was increased. We postulate that TSP-1, bound to the extracellular matrix (Galvin et al., 1987; Krutzsch et al., 1999; Panetti et al., 1999) did not dissolve into the supernatant, and/or that different culture conditions such as the concentration of EGF (Soula-Rothhut et al., 2004) and/or glucose (Wang et al., 2004) affect the expression of TSP-1.

Immunohistochemically, VEGF and Flt-1 were expressed in all the samples we examined; KDR was not expressed in any of our samples. This indicates that neither VEGF nor Flt-1 is a major factor in neovascularization after COE transplantation.

While normal corneal and oral epithelium expressed bFGF, CCE and COE did not. In vivo, bFGF binds to constituents of the extracellular matrix such as heparin sulfate (Van Setten et al., 1995; Okada-Ban et al., 2000). However, in vitro, the constituents of the epithelial extracellular matrix, particularly in the basement membrane, are different. While we did not examine whether bFGF was expressed in transplanted epithelial sheets, we postulate that its expression increases

post-transplantation due to factors such as inflammation and mechanical stress.

Although our earlier histological and electron-microscopic studies disclosed that COE and CCE manifest similar characteristics (Nakamura et al., 2004b), the current study revealed that they differ with respect to the expression of anti-angiogenic factors, particularly TSP-1. We postulate that this difference may be one of the causes of superficial peripheral neovascularization observed after COE transplantation. Further investigations regarding the inhibitory effects of TSP-1 on this neovascularization are needed.

Acknowledgement

The authors thank Kenichi Endo for assisting with Western blot analysis.

References

Castle, V.P., Dixit, V.M., Polverini, P.J., 1997. Thrombospondin-1 suppresses tumorigenesis and angiogenesis in serum- and anchorage-independent NIH 3T3 cells. Lab. Invest. 77 (1), 51–61.

Chang, J.H., Gabison, E.E., Kato, T., Azar, D.T., 2001. Corneal neovascularization. Curr. Opin. Ophthalmol. 12 (4), 242–249.

Cursiefen, C., Masli, S., Ng, T.F., 2004. Roles of thrombospondin-1 and -2 in regulating corneal and iris angiogenesis. Invest. Ophthalmol. Vis. Sci. 45 (4), 1117–1124.

Dawson, D.W., Volpert, O.V., Gillis, P., et al., 1999. Pigment epithelium-derived factor: a potent inhibitor of angiogenesis. Science 285 (5425), 245–248.

Galvin, N.J., Vance, P.M., Dixit, V.M., Fink, B., Frazier, W.A., 1987. Interaction of human thrombospondin with types I-V collagen: direct binding and electron microscopy. J. Cell Biol. 104 (5), 1413–1422.

Gipson, I.K., Geggel, H.S., Spurr-Michaud, S.J., 1986. Transplantation of oral mucosal epithelium to rabbit ocular surface wounds in vivo. Arch. Ophthalmol. 104, 1529–1533.

Iruela-Arispe, M.L., Lombardo, M., Krutzsch, H.C., Lawler, J., Roberts, D.D., 1999. Inhibition of angiogenesis by thrombospondin-1 is mediated by 2 independent regions within the type 1 repeats. Circulation 100 (13), 1423–1431.

Koizumi, N., Inatomi, T., Quantock, A.J., Fullwood, N.J., Dota, A., Kinoshita, S., 2000a. Amniotic membrane as a substrate for cultivating limbal corneal epithelial cells for autologous transplantation in rabbits. Cornea 19, 65–71.

Koizumi, N., Fullwood, N.J., Bairaktaris, G., Inatomi, T., Kinoshita, S., Quantock, A.J., 2000b. Cultivation of corneal epithelial cells on intact and denuded human amniotic membrane. Invest. Ophthalmol. Vis. Sci. 41, 2506–2513.

Koizumi, N., Inatomi, T., Suzuki, T., Sotozono, C., Kinoshita, S., 2001. Cultivated corneal epithelial stem cell transplantation in ocular surface disorders. Ophthalmology 108, 1569–1574.

Krutzsch, H.C., Choe, B.J., Sipes, J.M., Guo, N., Roberts, D.D., 1999. Identification of an alpha (3) beta (1) integrin recognition sequence in thrombospondin-1. J. Biol. Chem. 274 (34), 24080–24086.

Lin, H.C., Chang, J.H., Jain, S., et al., 2001. Matrilysin cleavage of corneal collagen type XVIII NC1 domain and generation of a 28-kDa fragment. Invest. Ophthalmol. Vis. Sci. 42, 2517–2524.

Ma, D.H., Yao, J.Y., Yeh, L.K., et al., 2004. In vitro antiangiogenic activity in ex vivo expanded human limbocorneal epithelial cells cultivated on human amniotic membrane. Invest. Ophthalmol. Vis. Sci. 45 (8), 2586–2595.

Morbidelli, L., Donnini, S., Chillemi, F., Giachetti, A., Ziche, M., 2003. Angiosuppressive and angiostimulatory effects exerted by synthetic partial sequences of endostatin. Clin. Cancer Res. 9 (14), 5358–5369.

Mumby, S.M., Abbott-Brown, D., Raugi, G.J., Bornstein, P., 1984. Regulation of thrombospondin secretion by cells in culture. J. Cell Physiol. 120 (3), 280–288.

Murthy, R.C., McFarland, T.J., Yoken, J., et al., 2003. Corneal transduction to inhibit angiogenesis and graft failure. Invest. Ophthalmol. Vis. Sci. 44 (5), 1837–1842.

Nakamura, T., Endo, K., Cooper, L.J., et al., 2003. The successful culture and autologous transplantation of rabbit oral mucosal epithelial cells on amniotic membrane. Invest. Ophthalmol. Vis Sci. 44, 106–116.

Nakamura, T., Inatomi, T., Sotozono, C., Koizumi, N., Kinoshita, S., 2004a. Successful primary culture and autologous transplantation of corneal limbal epithelial cells from minimal biopsy for unilateral severe ocular surface disease. Acta Ophthalmol. Scand. 82 (4), 468–471.

Nakamura, T., Inatomi, T., Sotozono, C., Amemiya, T., Kanamura, N., Kinoshita, S., 2004b. Transplantation of cultivated autologous oral mucosal epithelial cells in patients with severe ocular surface disorders. Br. J. Ophthalmol. 88 (10), 1280–1284.

Nakamura, T., Yoshitani, M., Rigby, H., et al., 2004c. Sterilized, freeze-dried amniotic membrane: a useful substrate for ocular surface reconstruction. Invest. Ophthalmol. Vis. Sci. 45 (1), 93–99.

Nishida, K., Yamato, M., Hayashida, Y., et al., 2004. Corneal reconstruction with tissue-engineered cell sheets composed of autologous oral mucosal epithelium. N. Engl. J. Med. 351 (12), 1187–1196.

Okada-Ban, M., Thiery, J.P., Jouanneau, J., 2000. Fibroblast growth factor-2 [Review]. Int. J. Biochem. Cell. Biol. 32 (3), 263–267.

Panetti, T.S., Kudryk, B.J., Mosher, D.F., 1999. Interaction of recombinant procollagen and properdin modules of thrombospondin-1 with heparin and fibrinogen/fibrin. J. Biol. Chem. 274 (1), 430–437.

Sekiyama, E., Nakamura, T., Cooper, L.J., Kawasaki, S., Hamuro, J., Fullwood, N.J., Kinoshita, S., 2006. Unique distribution of thrombospondin-1 in human ocular surface epithelium. Invest. Ophthalmol. Vis. Sci. 47 (4), 1352–1358.

Shao, C., Sima, J., Zhang, S.X., et al., 2004. Suppression of corneal neovascularization by PEDF release from human amniotic membranes. Invest. Ophthalmol. Vis. Sci. 45 (6), 1758–1762.

Soula-Rothhut, M., Coissard, C., Sartelet, H., et al., 2004. The tumor suppressor PTEN inhibits EGF-induced TSP-1 and TIMP-1 expression in FTC-133 thyroid carcinoma cells. Exp. Cell. Res. 304 (1), 187–201.

Tuszynski, G.P., Nicosia, R.F., 1996. The role of thrombospondin-1 in tumor progression and angiogenesis. Bioessays 18 (1), 71–76.

Van Setten, G.B., Fagerholm, P., Cuevas-Sanchez, P., 1995. Presence of basic fibroblast growth factor in corneal epithelium. Ophthalm. Res. 27 (6), 317–321.

Wang, S., Skorczewski, J., Feng, X., et al., 2004. Glucose up-regulates thrombospondin 1 gene transcription and transforming growth factor-beta activity through antagonism of cGMP-dependent protein kinase repression via upstream stimulatory factor 2. J. Biol. Chem. 279 (33), 34311–34322.